HUMAN VACCINES & IMMUNOTHERAPEUTICS
2020, VOL. 16, NO. 9, 2072–2091
https://doi.org/10.1080/21645515.2020.1775460

Taylor & Francis
Taylor & Francis Group

RESEARCH PAPER

OPEN ACCESS Check for updates

Cutaneous vaccination ameliorates Zika virus-induced neuro-ocular pathology via reduction of anti-ganglioside antibodies

Jacob T. Beaver[a], Lisa K. Mills[a], Dominika Swieboda[a], Nadia Lelutiu[a], Edward S. Esser[a], Olivia Q. Antao[a], Eugenia Scountzou[b], Dahnide T. Williams[a], Nikolaos Papaioannou[c], Elizabeth Q. Littauer[a], Andrey Romanyuk[d], Richard W. Compans[a], Mark R. Prausnitz[d], and Ioanna Skountzou[a]

[a]Department of Microbiology & Immunology, Emory University School of Medicine, Atlanta, GA, USA; [b]EyeVetSurgery-Small Animal Clinic, Athens, Greece; [c]Faculty of Veterinary Medicine, Laboratory of Pathologic Anatomy, Aristotle University of Thessaloniki, Greece; [d]Department of Biomedical Engineering, School of Chemical and Biomolecular Engineering, Georgia Institute of Technology, Atlanta, GA, USA

ABSTRACT

Zika virus (ZIKV) causes moderate to severe neuro-ocular sequelae, with symptoms ranging from conjunctivitis to Guillain-Barré Syndrome (GBS). Despite the international threat ZIKV poses, no licensed vaccine exists. As ZIKV and DENV are closely related, antibodies against one virus have demonstrated the ability to enhance the other. To examine if vaccination can confer robust, long-term protection against ZIKV, preventing neuro-ocular pathology and long-term inflammation in immune-privileged compartments, BALB/c mice received two doses of unadjuvanted inactivated whole ZIKV vaccine (ZVIP) intramuscularly (IM) or cutaneously with dissolving microneedle patches (MNP). MNP immunization induced significantly higher B and T cell responses compared to IM vaccination, resulting in increased antibody titers with greater avidity for ZPIV as well as increased numbers of IFN-γ, TNF-α, IL- and IL-4 secreting T cells. When compared to IM vaccination, antibodies generated by cutaneous vaccination demonstrated greater neutralization activity, increased cross-reactivity with Asian and African lineage ZIKV strains (PRVABC59, FLR, and MR766) and Dengue virus (DENV) serotypes, limited ADE, and lower reactivity to GBS-associated gangliosides. MNP vaccination effectively controlled viremia and inflammation, preventing neuro-ocular pathology. Conversely, IM vaccination exacerbated ocular pathology, resulting in uncontrolled, long-term inflammation. Importantly, neuro-ocular pathology correlated with anti-ganglioside antibodies implicated in demyelination and GBS. This study highlights the importance of longevity studies in ZIKV immunization, and the need of exploring alternative vaccination platforms to improve the quality of vaccine-induced immune responses.

ARTICLE HISTORY
Received 29 April 2020
Revised 19 May 2020
Accepted 23 May 2020

KEYWORDS
Zika virus; vaccination; neuro-pathology; auto-immunity

Introduction

The most severe consequence of adult Zika virus (ZIKV) infection is Guillain-Barré syndrome (GBS), a disease attacking peripheral nerves that can result in permanent neuro-ocular damage, such as macular degeneration.[1–3] As ZIKV and other flaviviruses persist up to 6 months in immune-privileged tissues such as brain, eyes, and genitals, these organs present a crucial focus for ZIKV vaccination research.[4–6] Indeed, ZIKV infections are spread via multiple modes of transmission; transplacentally to developing fetuses, via breastfeeding to infants, and through sex, or mosquito bite. Infants that acquire ZIKV often present congenital Zika syndrome (CZS), with impaired visual and neurological development. Most notable among these is microcephaly;, however, recent reports note instances of neuro-ocular pathology among infants independent of microcephaly.[7,8] The multi-modal transmission of ZIKV, coupled with its long-term persistence and impact on brain and eyes, underlies the importance of developing an effective vaccine with potential for worldwide distribution.

The production of autoantibodies in GBS leads to enhanced tissue pathology and clinical symptomatology. As such, progressive paralysis of one or more limbs culminating in hyporeflexia or areflexia are diagnostic hallmarks of GBS, and can be fully manifested within 4 weeks.[9] While other pathogens implicated in GBS, such as *Campylobacter jejuni*, develop pathology after pathogen clearance, ZIKV-induced GBS is initiated during infection.[10–12] Long-term demyelination of CNS tissues and chronic neuroinflammation is common among GBS patients, and have been linked to T cell infiltration into these tissues.[13,14] However, there is limited knowledge on the putative role of ZIKV-specific antibodies in initiating or sustaining neuro-ocular symptoms and the role that vaccination may play in their development.

Several publications have demonstrated the specific role of T cells in mediating brain pathology, such as synaptic degradation,[13] and detailed the role of retinal epithelial cells in maintaining ocular immune-privilege via blood-barrier integrity.[15,16] These studies often rely on a combination of human primary cell cultures and different mouse models. As flavivirus pathology is intricately linked to the host type I and type III interferon (IFN) response, many studies rely on short term observations in wild-type (WT) animals or utilize immunocompromised animals to generate extreme pathology. For

CONTACT Ioanna Skountzou iskount@emory.edu Department of Microbiology & Immunology, Emory University School of Medicine, Atlanta, GA 30322, USA
Supplemental data for this article can be accessed online at http://dx.doi.org/10.1080/21645515.2020.1775460.

example, Singh et al. provided a thorough transcriptional analysis of cellular responses after intra-ocular injection of ZIKV into either WT or ISG15 deficient C57BL/6 mice and demonstrated the rapid induction of inflammation in retinal cells.[15] This inflammation corresponded to retinal lesions within WT mice that persisted up to 96 hours after infection. Despite evidence that ZIKV-induced neuro-ocular pathology develops in a variety of murine models, few studies seek to evaluate the synergy between this pathology and humoral immune responses following vaccination.

There are at least 29 ZIKV vaccine candidates in various stages of clinical trials, with 45% of US-based candidates utilizing Zika virus inactivated particles (ZVIP)[17–21] in conjunction with adjuvants, administered subcutaneously (SC) or intramuscularly (IM).[22,23] These candidates are often are co-administered with an alum adjuvant.[19–21] In this study, we generated a Zika virus inactivated particle (ZVIP) vaccine using the Asian lineage PRVABC59 strain and implemented investigated two routes of delivery,: IM and or cutaneous with dissolving polymer microneedle patches (MNP) encapsulating the vaccine.[24–26] By targeting the cutaneous vaccine to epidermal keratinocytes, Langerhans cells, and dermal dendritic cells, we aimed to mobilize unique immunological mechanisms and signaling pathways from the vaccination site to draining lymph nodes, enhancing ZIKV-specific B and T cell responses.[27,28] We have previously demonstrated that MNP immunization confers superior immune responses compared to conventional IM vaccination in adult BALB/c mice,[29,30] and in high-risk populations.[31] Hence, we considered the MNP approach as more effective for a mosquito-borne infection because epithelial cells are early ZIKV infection targets[32] and protection can be conferred using skin-resident memory T cells.[33]

MNP immunization with ZVIP was juxtaposed to IM immunization to test our hypothesis whether vaccine delivery via the skin can induce potent, long-lasting, and broadly protective immune responses using an immunocompetent BALB/c mouse model. This strain was selected over C57BL/6 mice for its ability to generate robust humoral responses in vaccination studies and for the less invasive approach to generate neuro-ocular symptoms; while BALB/c mice can present pathology of these compartments following intravenous infection with ZIKV, C57BL/6 mice require intracranial injection in order to achieve similar ZIKV neuro-ocular pathology.[34] Here, we seek to build on existing vaccine candidates by using a prime-boost administration approach to investigate kinetics, magnitude, and quality of immune responses, evaluate if vaccination confers robust protection against infectious challenge, and to correlate reductions in auto-reactive antibodies and neuro-ocular pathology with vaccination routes.

Methods and materials

Cells and virus stocks

Vero cells (ATCC, CCL-81) for virus propagation and titration were maintained in DMEM (Mediatech, 10–013-CV) containing 10% fetal bovine serum (FBS; Hyclone, Thermo Scientific, SH3007103), HEPES (Corning, H3537) and 1% Penicillin/Streptomycin (Corning, 30–002-CI). ZIKV stocks were generated from the African lineage Uganda strain (MR766, B.E.I. resources, NR-50085) and the Asian lineage, Caribbean isolate from Puerto Rico (PRVABC59, generously provided by Dr. Scott Michael and Dr. Sharon Isern at Florida Gulf Coast University). The FLR strain from Colombia was obtained from B.E.I (B.E.I. resources, NR-50183). Resources. Dengue virus strains (DENV1/Hawaii/1944, DENV2/16681/Thailand/1964, DENV3/H87/Philippines/1956, and DENV4/UNC4019/Colombia/2006) were generously provided by Dr. Joshy Jacob of Emory University. All viruses were propagated in Vero cells for 7 days at 37°C. After the tenth passage, culture supernatants were collected and cell debris was cleared by centrifugation at 3,000xg for 10 minutes at 4°C. Viral harvest was then filtered using 0.22-micron filters (Sigma, Z741966). Culture supernatants were concentrated using Amicon centrifugal concentration filters (EMD Millipore, C7715) by centrifugation at 4,000xg for 30 minutes. As the ZIKV virion is approximately 50 nm in diameter, we used the 100 NMWL variant filters to maximize the recovery. Finally, viral supernatants were purified by discontinuous 20–60% sucrose gradient, where they were diluted 1:5 with FBS before final storage at −80°C.[35]

Virus titration

Viral stocks were titrated by plaque assay performed in Vero cells as previously described.[36] Focus-forming assays were performed as previously described.[37] Blue foci were counted, and titers were calculated by foci numbers in infectious volume (# of foci x infectious volume x conversion factor to ml x dilution factor). FFU and PFU are equivalent in that both are quantification methods. In this study, PFU assays and FFU assays resulted in similar titers.

Trans-well focus-forming assay

To evaluate if live virus can be isolated from systemic and privileged tissues and bodily fluids, we adapted a trans-well infectious system similar to a monocyte chemotaxis assay used for Japanese Encephalitis Virus.[38] Tissue homogenates and cell suspensions were then added onto 0.4 μm trans-well insert systems (Corning, CLS3396) overtop sterile Vero cells. Live virus released from cells in contact with the insert filtered through the membrane to infect permissive Vero cells below to provide a measure of tissue-specific live viral load as opposed to quantifying the amount of vRNA present in tissues.

Vaccine preparation

ZIKV-PRVABC59 stocks were prepared as detailed above and were titrated with plaque assay and FFA.[36] Viral stocks were inactivated with 0.04% formalin for 7 days at 22°C and subjected to membrane dialysis[39] to remove formalin.[40] Stocks were then tested for successful inactivation by plaque assay and FFA in Vero cells.

ZIKV incorporation into MNP

MNPs were fabricated and underwent quality control testing as previously described.[41] Briefly, MNPs containing the vaccine

were dissolved in PBS, ran on a 10% SDS-PAGE gel and immune-stained with anti-ZIKV E-protein antibody (EMD Millipore, MAB10216) in order to visualize protein bands and to determine successful incorporation of the inactivated virus. MNPs were fabricated in a two-step process with polydimethylsiloxane (PDMS) molds as previously described.[42] MNPs were prepared by sequentially casting the first-cast solution to fill the mold cavities and the second-cast solution to cover the mold surface (corresponding to the MNP patch backing). The MN patches were removed from the molds and attached to adhesive paper discs. Patches were inspected via light microscopy for integrity and uniformity

Animal strains and housing

Female BALB/c mice (Charles River Laboratories) were housed in a biosafety level 1 facility at Emory University's Division of Animal Resources and viral infection experiments were performed on animals housed in a Biosafety Level 3 facility at Emory University's Division of Animal Resources. All experiments were conducted in accordance with protocols (DAR2002950-122617BN) approved by Emory University's Institutional Animal Care and Use Committee (IACUC) and in accordance with guidelines with the United States Federal Animal Welfare Act (PL 89–544) and subsequent amendments. At the time of vaccination, mice were 5–6 weeks old.

Vaccination protocol

BALB/c mice were vaccinated with 4 μg of whole, inactivated ZIKV. Vaccine was administered via MNP[43] or IM injections using a prime-boost vaccination schedule. Mice were anesthetized using a ketamine/xylazine cocktail, and MNP patches were administered to the caudal side of the dorsum using direct pressure for 1 minute, and then left for 20 minutes.[27] Thirty days after prime vaccination, mice received an identical booster immunization, and were then infected 30 days later. Antibody kinetics were performed on days 7 and 30 post-prime vaccination, and again on days 7, 14 and 30 post-booster vaccination.

Animal infection, tissue and biological fluid sampling

Mice were infected with 1×10^6 FFU of ZIKV-PR virus intravenously (IV).[44] Serum or platelet-poor plasma (PPP) was collected 0, 3, 6, 10, 30, 40, 60, 80, 100, and 120 days post-challenge; plasma was collected in citrate buffer and stored at −20°C until use. Small groups of mice were euthanized at 10 and 100 DPI. Tissues were collected and processed for histology, homogenized in protease inhibitors and RNase inhibitors (ThermoFisher Scientific, Waltham, MA) for infectivity and qRT-PCR studies. In the remaining mice, tears were collected via PBS gavage 100 DPI and after euthanasia. Tissues (brain, eyes, genital organs, liver and spleen) were collected and processed for infectivity experiments, histology, and inflammatory markers. Ocular tissues were not perfused prior to harvest to avoid structural and cellular changes induced by the perfusion process,[45] as functional morphology of the retina correlates directly with fluid pressure in the choroid. For both FFA and qRT-PCR quantification methods, tissues were homogenized after mincing and passaged through 40 μm cell strainers (Fisher Scientific, 08–771-1). They were further digested with 1 mg/ml of Collagenase IV (Worthington, LS004189) for 30 minutes at 37°C, and the purified through 40 μm cell strainers. Homogenates were separated using a Percoll (Millipore Sigma, P1644) density gradient,[46,47] and cell suspensions were isolated for qRT-PCR and FFA trans-well studies. One eye from each animal was used for FFA and qRT-PCR experiments, and the other was used for tissue sectioning for microscopy studies.

RNA isolation and qRT-PCR

Total RNA was extracted from tissues using Trizol (Ambion, 15596018). Tissues were homogenized into Trizol reagent using the FastPrep-24 5 G homogenizer (MP Biomedicals). Total RNA was isolated using the PureLink RNA mini-kit (Ambion, 12183025). Purified RNA was quantified, checked for quality assurance via NanoDrop Spectrometry (ThermoFisher, ND200), and then reverse transcribed with the qScript Reverse Transcription kit (QuantaBio, 95047). For quantification of vRNA, a standard curve was generated using 10-fold serial dilutions of ZIKV RNA standard. qRT-PCR for ZIKV prM-E was performed with TaqMan Gene Expression Master Mix, ZIKV Primers, and probe as previously described.[48] The standard curve had an R^2 value greater than 0.99. vRNA copies were interpolated from the standard curve using the average Ct value obtained from samples run in triplicate. qRT-PCR for GAPDH, IL-1β, TNF-α, IL-10, SOCS3, MMP2, MMP9, and COX2 were performed with PerfeCTa SYBR Green SuperMix Low Rox (Quantabio, #95056-500). Primers for GAPDH, IL-1β, TNF-α, IL-10, SOCS3, and COX2 were as previously described.[49] MMP2 primers were as follows; forward 5′-AACGGTCGGGAATACAGCAG-3′; reverse 5′-GTAAAC AAGGCTTCATGGGGG-3′. MMP9 primers were as follows; forward 5′-AACCTCCAACCTCACGGACA-3′; reverse 5′-AGGTTTGGAATCGACCCACG-3′. Data was analyzed using the ΔΔCt method to determine normalized relative expression.

Ocular and brain symptomatology

At the same time points of blood collection post-infection, animals were assessed for ocular and motor/neural symptomatology. Behavioral tests to characterize pathogenesis in our mouse model were adapted from the Department of Molecular & Comparative Pathobiology's 2015 Lab Manual from Johns Hopkins University School of Medicine.[50] These assessments were identified and further researched with the explicit aim to evaluate visual and motor function following ZIKV infection.

Visual placement reflex

A reaching reflex test, or visual placement assessment measures optic function and can also potentially indicate inflammation in parietal and occipital lobes of the brain.[51,52] It is performed by holding the mouse gently by the tail suspended approximately 1–2 feet above a solid cage grate surface.[50] The mouse is

then vertically lowered slowly toward the grate, taking note not to allow whiskers to contact the surface. A mouse with normal, average visual capabilities will attempt to reach toward the surface. A mouse that is blind, with impaired vision, or spatio-temporal problems will not attempt to reach until the whiskers contact the surface. Alternatively, the impaired mouse may also try to bend backwards on itself, in attempt to right itself using its awareness of gravity.

Palpebral reflex

Alternatively called the corneal reflex, it measures optic function and indicates potential inflammation in central nervous tissue connected to the optic tract, such as the trigeminal nerve, occipital lobe, and parietal lobes of the brain.[53,54] It is performed by using a teased-out cotton tipped applicator. The mouse is held steady, and the cotton is gently touched against the cornea.[50] The blinking response is assessed on a scale of 0 to 3. On this scale, 3 represents a hyper-repetitive blinking in response to corneal stimulation; 2 equivocates to a normal, quick blink response; 1 corresponds to a slow blink or a closure response to stimuli; and a score of 0 indicates there was no response to corneal stimuli. Impaired or absent reflex responses suggests deteriorated motor/neural capabilities, eye function, and potential neurological inflammation.

Rear limb withdrawal

The limbic withdrawal test measures motor neuron responses in mice, and can indicate arthralgia in limb joints, and/or inflammation of motor neurons.[55,56] The mouse is allowed to grip onto a surface and steadied by the tail.[50] One of the hind limbs is gently picked up and pulled taut at a 45° angle. The limb is then released, and the withdrawal of the limb is scored on a scale 0 to 3. On this scale, 3 represents a hyper-active response; 2 equivocates to a normal quick withdrawal of the limb back to normal position; 1 corresponds to a slow response to stimulus; and a score of 0 indicates there was no response, and leg drops to the ground and does not return to normal position.

Grip time assessment

The grip time assessment quantitatively evaluates mouse muscular capabilities and indicates potential arthralgia and muscular coordination issues.[57,58] The test was performed by placing a mouse on a grated cage lid, and the grate was suspended 1–2 feet above the bench-top or cage.[50] The mouse and grate were gently shaken for 1 minute, and then rapidly inverted to bring the mouse into an upside-down position. The time the mouse could successfully hold on without falling off the grate was recorded. Healthy mice are expected to be able to hold onto the grate for a minimum of 1 minute. Any recordings less than 60 seconds were considered abnormal.

Histopathology and immunofluorescence of eyes and brain

To evaluate tissue infectivity, viral burden, and infection-induced histopathology, eyes and brains were harvested from 5 out of 20 total mice per group at 10 and the remaining at 100 DPI. The tissues were fixed in 10% formalin solution, followed by paraffin embedding for 8 μm sectioning. Sectioning of brain tissues was performed at the Neuropathology/Histochemistry core of the Emory NINDS Neurosciences Core Facility (P30 NS055077), sectioning and H&E staining of eye tissues was performed by the L.F. Montgomery Ophthalmology Pathology core.

Immunofluorescent staining

Slides were de-waxed and rehydrated using sequential washes of xylene, ethanol, and distilled water. Antigens were unmasked and retrieved by submersion in sodium citrate buffer (10 mM, pH 6.0) for 10 minutes at 56°C. Aldehyde auto-fluorescence was quenched in a humidified chamber using 3 M glycine solution, and lipofuscin auto-fluorescence was quenched using Sudan-Black B. Slides were then blocked in bovine serum albumin (2% BSA)-TBS. Primary antibody diluted in 1% BSA in PBS buffer was added directly on top of each section, and slides were incubated overnight at 4°C. The 4G2 antibody (Millipore, MAB10216) was used for viral infectivity analysis. Myelination studies utilized anti-MBP-Alexa Fluor488 (SantaCruz, sc-271524), anti-Vimentin (Abcam, ab92547), and anti-Myelin PLP (Abcam, 28486) antibodies. Secondary antibodies were fluorescently conjugated (Anti-Mouse Alexa594, Biolegend #405326; Anti-rabbit Alexa547, Abcam, ab150167; Anti-mouse Alexa488, Invitrogen, A10667), diluted in 1%BSA in PBS solution and incubated for 2 hours at room temperature. Prolong Gold Antifade mounting medium with DAPI (Thermo-Fisher, P36931) was applied, and slides were covered with a coverslip. Images were taken on Zeiss AxioScope microscopes via SPOT-advanced imaging software. Images were processed in Fiji/ImageJ.

TUNEL staining

TUNEL stain was selected because for the broad range of cell death pathways it stains for, i.e. apoptosis, necrosis, and pyroptosis.[59–61] While there is no definitive way to discern between these pathways via TUNEL stain, DNA fragmentation does occurs in all of these cell death pathways, making it preferable in this study where we seek to identify cell death induced by infection rather than specific pathways. Terminal deoxynucleotidyl transferase dUTP nick end labeling, or TUNEL, staining was performed according to manufacturer protocol (Abcam, ab66110). Slides were de-waxed and rehydrated using sequential washes of xylene, ethanol, and distilled water. Antigens were unmasked and retrieved by submersion in sodium citrate buffer (10 mM, pH 6.0) for 10 minutes at 56° C. Aldehyde auto-fluorescence was quenched in a humidified chamber using 3 M glycine solution, and lipofuscin auto-fluorescence was quenched using Sudan-Black B. Slides were then blocked in bovine serum albumin (2% BSA)-TBS. Slides were then washed in PBS and blocked using a proteinase K solution for 5 minutes at room temperature. Wash slides with PBS and then label fragmented DNA using TdT enzyme, enzyme buffer, and Br-dUTP (Abcam, ab66110). Prolong Gold Antifade mounting medium with DAPI (Thermo-Fisher, P36931) was applied, and slides were covered with a coverslip. Images were taken on Zeiss AxioScope microscopes via SPOT-advanced imaging software. Images were processed in Fiji/ImageJ.

Quantification of MBP, Myelin PLP, and 4G2 positive cells

Corrected total cellular fluorescence (CTCF, also called normalized MFI) was determined as described by Lourenço et al. for both MBP, myelin PLP, and vimentin stains.[62] Similarly, to determine the percentage of 4G2 positive cells, DAPI foci and 4G2 cells were enumerated both manually and automatically, using the "Threshold" and "Analyze particles" functions in FIJI/ImageJ. The percent of infected cells was then calculated as the number of 4G2 positive cells was divided by the number of DAPI positive foci.

Antibody titration and characterization

ELISAs

Anti-ZIKV specific antibodies were determined by coating flat bottom, 96-well Nunc MaxiSorp plates (Thermo-Fisher, 44–2404-21) with 4 μg/ml of inactivated virus stocks, diluted in sodium bicarbonate buffer. Plates were incubated overnight at 4°C, washed with PBS-Tween 0.5%and blocked with 2% BSA in PBS for 1 hour. Individual PPP samples were run in duplicate and incubated for 2 hours at 37°C. The standard curves were generated with appropriate purified mouse immunoglobulins and isotype-specific HRP-labeled detection antibodies (Southern Biotech, Birmingham, AL). Sample IgG concentrations were determined by interpolation from standard curves. Anti-ganglioside specific antibody concentrations were determined similarly. Flat bottom, 96-well Nunc MaxiSorp plates were coated with 2 μg/ml of either GD1a, GD1b, or GT1a ganglioside (SantaCruz, sc-202621, sc-202622, sc-202629, respectively). Standard wells were coated as described above. PPP samples were diluted. Standard curve antibodies and development of plates was performed as described previously.[63] The avidity index was determined using Prism 7.03 Software (GraphPad, La Jolla, CA) by calculating the molar concentration of the chaotropic agent required to reduce the initial optical density by 50% as previously described.[63]

Focus-forming reduction by neutralization assay (FFRNT)

Heat-inactivated PPP samples were diluted serially and combined with 100 FFU live virus. Antibody dilutions and virus were co-incubated for 1 hour at 37°C, and then added over Vero cells for 24 hours. The focus-forming assay was performed as described.[37]

Avidity

Competitive ELISA with chaotropic inhibition was performed as described previously.[63]

Flow cytometry identification of activated cellular subsets

Skin draining (inguinal) lymph nodes were collected at 7 and 14 DPV to evaluate the presence of activated T_{FH} cells, $CD8^+$ follicular cells, and GC B-cells. Spleens were also collected at 7 and 14 DPV (−53 and −46 DPI) to evaluate the presence of recently activated T-cell populations, as well as for differentiated B-cell subsets.[41] Samples were acquired on an LSR II flow cytometer (BD Biosciences) and data were analyzed with FlowJo (FlowJo LLC, BD, v9.9) (Gating strategies available in SFigure 2A, B, and C).

ELISpot

ELISpot assays were performed and quantified as described previously.[63]

Antibody-dependent enhancement assay

ADE assay protocol was performed as described using U937 cells.[37] The cells were maintained in suspension in complete RPMI medium. Cells were stained with 4G2 antibody (EMD Millipore). Samples were run on a CytoFLEX LX system at Pediatrics/Winship Flow Cytometry Core of Winship Cancer Institute of Emory University, Children's Healthcare of Atlanta and NIH/NCI, which is supported under the award number P30CA138292.

Statistical analysis

Correlation analysis was performed on vRNA titers determined by qRT-PCR for brain and eyes to determine a relationship with raw reflex scores. Pearson's correlation coefficient with a two-tailed *p*-value were calculated for each of the four reflexes. For ELISA assays, linear regression tests to interpolate OD values into concentrations. For ELISPOT, flow cytometry, co-culture assays, and qRT-PCR, two-way ANOVA followed by Bonferroni's Post Hoc test for multiple comparisons was used to analyze differences between vaccination groups, as well as between vaccinated and unvaccinated groups following infection. Two-way ANOVA with Bonferroni's post-hoc was also used to determine differences between uninfected and infected groups, as well as between vaccination groups for all reflex assessments performed. For immunofluorescence assays, two-way ANOVA was used to compare difference hippocampal and cortical regions, as well as between early and late timepoints. Non-linear regression analysis was performed to determine the IC_{50} (95% confidence interval) for avidity and neutralization assays. A *p*-value less than 0.05 was considered significant.

Results

MNP vaccination induced a greater concentration of vaccine-specific antibodies with higher avidity

he role of autoreactive $CD8^+$ T cells has been well documented in regard to ZIKV neurological pathology, but the putative interplay of autoantibodies has been neglected despite the obvious connection between self-reactive antibodies and GBS.[13] Here, we utilized two vaccination strategies to investigate their effect on antibody magnitude, quality, and protective immunity against viral infection. Two cohorts of mice were vaccinated as per the schematic in Supplementary Figure 1A using either intramuscular injection (IM), cutaneously delivery using dissolving polymer microneedle patches (MNP), or an empty MNP as a mock vaccination control. All animals received a primary vaccination of 4 μg of ZVIP injected either by IM or MNP, and were then monitored for 30 days. After 30 days, animals received a booster vaccination that was identical to the prime in both dose and administration route, and subsequently monitored for an additional 30 days.

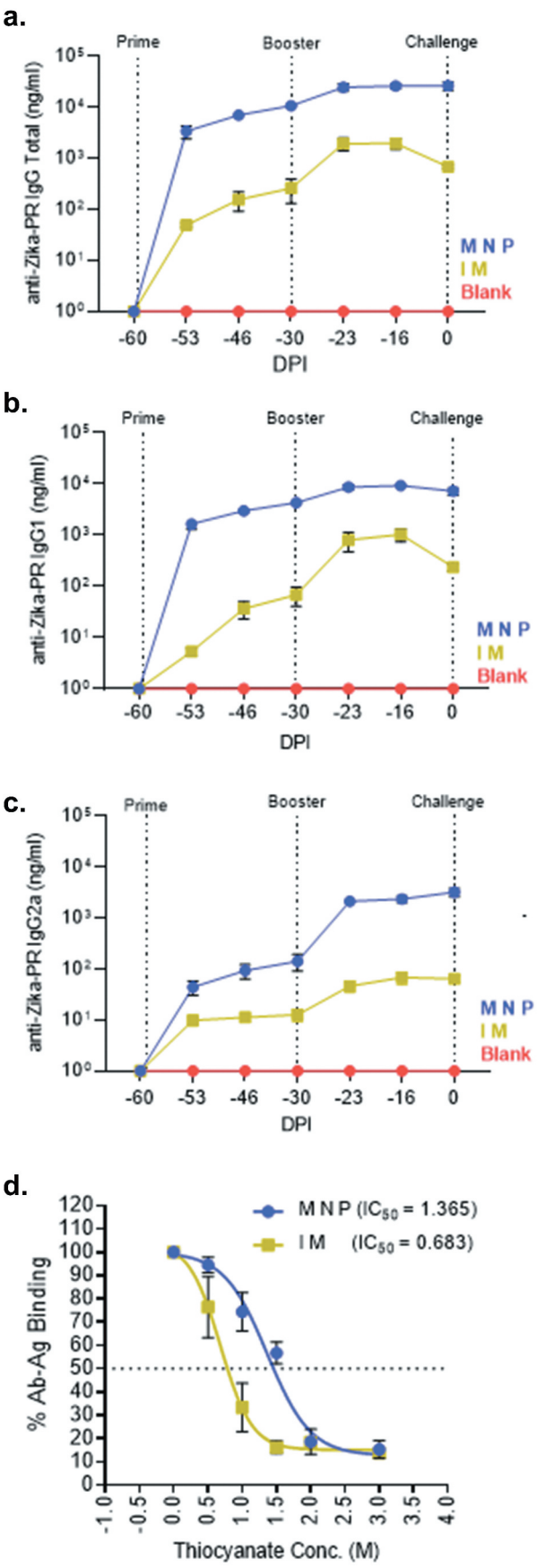

Figure 1. Cutaneous vaccinations induced greater antibody concentrations that bind with higher avidity. Animals received a prime vaccination 60 days prior to infectious challenge (−60 DPI) by either IM or MNP, and were then monitored 7 and 14 days after vaccination (−53 and −46 DPI). Animals received a duplicate vaccination that was identical in route and dosage, termed booster, 30 days after vaccination (−30 DPI). After booster vaccination, animals were again monitored 7 and 14 days (−23 and −16 DPI). Vaccine-specific IgG total (a), IgG1 (b), and IgG2a (c). Vertical lines denote prime and booster vaccination administration and also identify 0 DPI as the day animals were challenged. (All N = 10) (d) Antibody avidity was determined by chaotropic competitive ELISA (N = 10). The dotted horizontal line denotes the IC_{50}, or the concentration of thiocyanate needed to remove 50% of antibodies bound to vaccine-antigen. Antibody-antigen binding (Ab-Ag) is analyzed using a non-linear analysis (Log (inhibitor) vs response with a variable slope) to determine the logIC_{50}. Error bars represent standard deviation for all panels.

Prior to all vaccination experiments, ZVIP incorporation into the MNPs was confirmed qualitatively by microscopy to visualize ZVIP vaccine combined with sulforhodamine dye and by Western blot (Fig S1B). Patches with – vaccine mixed with vital dye (sulforhodamine) are pictured after patch casting and after needle dissolution in porcine cadaver skin (Fig SB-i and ii, respectively) Vaccine delivery into porcine cadaver skin was verified by the presence of dye deposition (Fig S1B-iii). Vaccine concentration in the new patches and used patches was quantitatively estimated with sandwich ELISA. The difference in concentration between new and used patches allowed us to calculate the percentage of vaccine delivery in the skin and thus adjust the dose to match those delivered with needle and syringe. MNPs are simple-to-administer skin patches that contain water-soluble, solid, conical needles of microns dimensions that encapsulate vaccine.[24–26] Upon painless application to skin, the microneedles dissolve and release the vaccine within minutes, after which the used patch can be discarded as non-sharps waste. To ensure the ZVIP vaccine was successfully incorporated in patches, we ran a western blot to confirm the presence of ZVIP in cast patches (SFig1-Biv).

Antibody kinetics of ZVIP-specific IgG, IgG1, and IgG2a were evaluated by ELISA (Figure 1). MNP vaccination generated at least 10-fold greater total IgG as early as 7 days after vaccination (−53 DPI) compared to IM vaccination (Figure 1a). MNP-induced total IgG concentrations remained 10-fold greater for all time-points prior to infectious challenge. IgG1 induced by MNP showed an immediate spike of antibodies, followed by a plateau of concentration for the remaining time-points. IM-induced IgG1 showed a gradual increase in titer concentration that increased further after the booster vaccination (Figure 1b). MNP and IM vaccinations demonstrated similar kinetic trends for IgG2a concentrations, but MNP vaccine recipients had consistently 4.4- to 50-fold greater concentrations of IgG2a than IM vaccinated mice (Figure 1c). Prior to infectious challenge, 30 days after booster vaccination (0 DPI), we measured antibody avidity as an index of antibody maturation and quality (Figure 1d). MNP generated antibodies demonstrated IC_{50} of 1.365 M, and IM antibodies had an IC_{50} of 0.683 M, a 2.2-fold difference (p = .023). This data demonstrates that MNP patches induce greater concentrations of vaccine-specific antibodies, and that after a prime and booster vaccination animals that received MNPs have antibodies with greater avidity for vaccine-antigen.

MNP vaccinations induced sustained B and T cell responses while IM vaccination induced ephemeral T cell secretory responses

ZVIP-specific $CD8^+$ and $CD4^+$ T cells impact viral pathogenesis and have established roles in autoreactive demyelination and chronic neuroinflammation; as such, cellular responses after a single vaccination were also evaluated. The frequency of germinal center (GC) B cells, follicular helper T cells (T_{FH}), follicular $CD8^+$ T cells, and $CD4^+$ and $CD8^+$ cells in inguinal lymph nodes (ILN) and spleen suspensions were quantitated (gating strategies in Fig S2). $CD19^+CD3\varepsilon^-GL7^+FAS^+$ ILN GC B cell levels were 10-fold higher in ZVIP-MNP than IM groups as early as 7 days post-vaccination (DPV; −53 DPI) (Figure 2a–i) and 20-fold higher by 14 DPV (−46 DPI) ($p < .0001$, $p = .02$

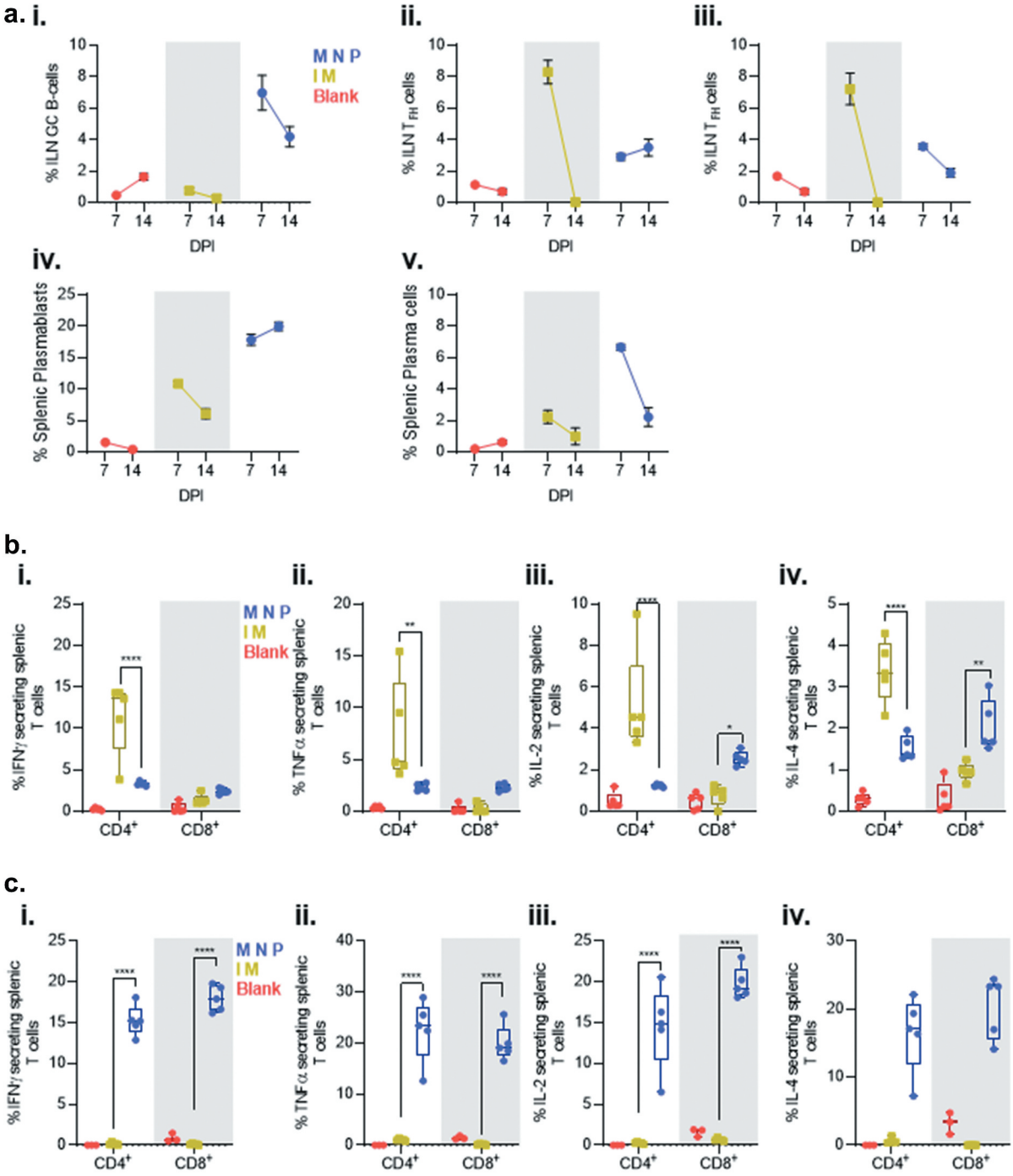

Figure 2. Cutaneous vaccination generated greater B and T cell responses within 2 weeks after of vaccination. (a) Kinetics of cellular responses to a single vaccination were evaluated in immune competent female BALB/c mice 7 and 14 DPV (−53 and −46 DPI). Germinal center B cell (i), T_{FH} cell (ii), and follicular $CD8^+$ cell (iii) kinetics were evaluated in inguinal lymph nodes, ILN, (N = 10 for −53 DPI; 5 for −46 DPI). Splenic plasmablasts (iv) plasma cell frequencies (v) were also evaluated for systemic humoral responses (N = 5 for −53 and −46 DPI). Two-way ANOVA test was used to compare vaccine administration routes between vaccination groups and corrected using Sidak post-host analysis. $CD4^+$ and $CD8^+$ T cell subsets at 7 (b) and 14 (c) days post prime vaccination (−53 and −46 DPI) were analyzed for secretion of IFNγ (i), TNFα (ii), IL-2 (iii), and IL-4 (iv) (N = 5). Two-Way ANOVA test was used to compare vaccine administration routes and corrected using Sidak post-host analysis. For all panels, * is $p < .05$, ** is $p < .01$, *** is $p < .001$, and **** is $p < .0001$. Error bars represent standard deviation for all panels.

respectively). The frequencies of TCRβ$^-$/B220$^+$/CD138$^+$ splenic plasmablasts were 2-fold 7 DPV (−53 DPI) and 3-fold 14 DPV (−46 DPI) higher in the MNP group compared to IM ($p < .0001$) (Figure 2a–iv and v). TCRβ$^-$/B220$^-$/CD138$^+$ splenic plasma cells were 3-fold 7 DPV (−53 DPI) and 2-fold 14 DPV (−46 DPI) in the MNP group compared to the IM group ($p < .0001$).

IM immunization elicited an early, significant spike of CD19$^-$/CD3ε$^+$/CD4$^+$/CXCR5$^+$/PD-1$^+$CD4$^+$ and CD19$^-$/CD3ε$^+$/CD8$^+$/CXCR5$^+$/PD-1$^+$CD8$^+$ follicular T cell frequencies. At 14 DPV (−46 DPI), follicular T cell subsets contracted 10-fold in IM vaccinees from 10% to <1% but remained constant at 3% in MNP vaccinees (7 DPV $p < .0001$; 14 DPV $p = .0019$; −53 DPI $p = .0001$) (Figure 2a–ii and iii). IFN-γ, IL-2, IL-4, or TNF-α secretion among CD4$^+$ T cells was 3-fold greater in IM than MNP groups 7 DPV (−53 DPI; $p < .0001$, $p = .0013$) (Figure 2b). By 14 DPV (−46 DPI), MNP immunization increased the frequency of CD4$^+$ T cells secreting IFN-γ by 87.1-fold, TNF-α 21.7-fold, IL-2 53.4-fold, and IL-4 26.1-fold (all $p < .0001$) (Figure 2c), suggesting delayed activation of CD4$^+$ T cells due to an antigen-depot effect.[27] MNP-induced CD8$^+$ T cell secretion was low 7 DPV (−53 DPI) but was still 7- to 10-fold higher than IM (IFN-γ $p = .0026$; TNF-α $p < .0001$; IL-2 $p < .0001$; IL-4 $p = .0018$) (Figure 2b). Importantly, IM vaccination-induced CD8$^+$ T cells were indistinguishable from blank vaccinated controls, while MNP vaccination-induced CD8$^+$ secreting cells were 16–25% greater than IM groups (all $p < .0001$) (Figure 2b).

Overall, our data suggests that MNP vaccination induces greater cellular responses in addition to ZVIP-specific antibodies of superior immunological quality. Systemic vaccination appears to offer an ephemeral CD4$^+$ T cell response that does not persist beyond 7 DPV (−53 DPI), whereas MNP vaccination not only induces elevated and persistent CD4$^+$ and CD8$^+$ T cells in LN and spleen, but that these populations expand continually after vaccination.

Unadjuvanted IM vaccination offered little protection against infectious challenge

Animals were challenged with live virus that was homologous to the vaccine strain 30 days after receiving a booster vaccination. To evaluate vaccine protective efficacy, weight changes were monitored post-challenge up to 120 DPI; both MNP and IM vaccination protected against weight loss (Figure 3a). MNP vaccinees did not lose weight after infection and IM vaccinees lost a maximum of 5% of their starting weight 6 DPI. Blank controls showed 10% weight loss 6 DPI, followed by a slow recovery of weight (Figure 3a).

As ZIKV has demonstrated persistence in human organs and fluids for ≥200 days,[64] we evaluated viral burden in brain, eyes, and plasma 10 and 100 DPI. Thus, we quantified viral burden in tissues and secretions with a focus-forming assay (FFA) co-culture, where homogenized tissues were used in a trans-well system over permissive Vero cells.[38] Homogenized tissues shed live virus through the membrane pores, infected permissive sterile cells below, and provided FFU/ml for each tissue. Homogenates were not added directly to monolayers because this does not discriminate if the cells are permissive to infection and a productive infection. Previous concerns were raised that ZIKV would not propagate in WT BALB/c tissues due to STAT non-homology. Thus, they were evaluated here to specifically identify if live virus was being shed from the tissues. Compared to IM vaccinations, MNP-vaccinees co-cultures exhibited 10- and 15-fold lower viral load for brains and eyes, 24- and 13-fold less for spleen and liver, and 11-fold less for tears and plasma at 100 DPI (all $p < .0001$) (Figure 3b). qRT-PCR quantification of vRNA mirrored FFA co-culture findings, where MNP vaccinations showed 6.4-, 3.6-, and 4.1- fold less vRNA in brain, eyes, and plasma, respectively at 100 DPI ($p \leq 0.0001$ for all groups) (Figure 3c).

The development and severity of neurological and ocular pathology was assessed by clinical reflexes up to 120 days after infectious challenge. For palpebral reflexes, MNP recipients exhibited a nadir at 10 DPI, with approximately 60% of animals showing loss of palpebral reflex ($p = .0013$ for 6 DPI, $p < .0001$ for all other time-points), while blank controls show a nadir at 6 DPI (Figure 3d). After this sharp decline, symptoms waned and animals recovered, with only 10% of animals demonstrating hyporeflexia at 120 DPI. IM recipients showed an immediate impairment in reflexes, with 45% of animals showing areflexia as early as 3 DPI, with the lowest score at 10 DPI, and long-term persistence up to 120 DPI. MNP vaccinees showed minimal loss of visual placement reflex, with only 15% of animals showing areflexia in a cyclical pattern, potentially indicating host inability to control viremia long-term and a periodic reemergence of virus from privileged compartments. In contrast, IM vaccination resulted in a 50% impairment of visual placement reflex within 6 DPI, with 70% of animals showing areflexia at 30 DPI, and persistent loss of visual placement abilities up to 120 DPI (all $p < .0001$) (Figure 3e).

Rear limb withdrawal kinetics showed a trend similar as that observed with palpebral reflex, where MNP vaccinated animals demonstrated the maximum loss of reflex ability 10 to 30 DPI with approximately 40% showing hyporeflexia (Figure 3f). Of these, 30% exhibited a partial recovery and ultimately only 10% had persistent hyporeflexia 120 DPI. In contrast, IM vaccinated mice showed two negative peaks at 10 and 40 DPI, with 65% of animals suffering from hyporeflexia (6 DPI $p = .01$; 10 DPI $p = .0014$; 40 DPI $p = .0004$; 80, 100 and 120 DPI $p < .0001$). These animals underwent a periodic cycle of convalescence and reemergence of symptoms, and 60% of them showed persistent loss of withdrawal reflexes (Figure 3f). Finally, IM and MNP recipients demonstrated 2.8- and 2.1-fold lower grip times 6 DPI, respectively, with MNP vaccine recipients showing a gradual recovery across the time-course and reaching normal scores by 60 DPI. IM vaccinated animals, on the other hand, maintained reduced grip times significantly lower than uninfected/blank vaccinated control group until 100 DPI (40 DPI $p = .0002$; 60, 80, and 100 DPI $p < .0001$) (Figure 3g).

IM vaccination exacerbated intraocular pathology without protecting against infection or cell death

Ocular pathology was evaluated 10 and 100 DPI in IM, MNP, and uninfected/blank vaccinated animals. After 10 days, IM and blank recipient mice demonstrated stromal inflammation, corneal destruction, complete loss of corneal cellular

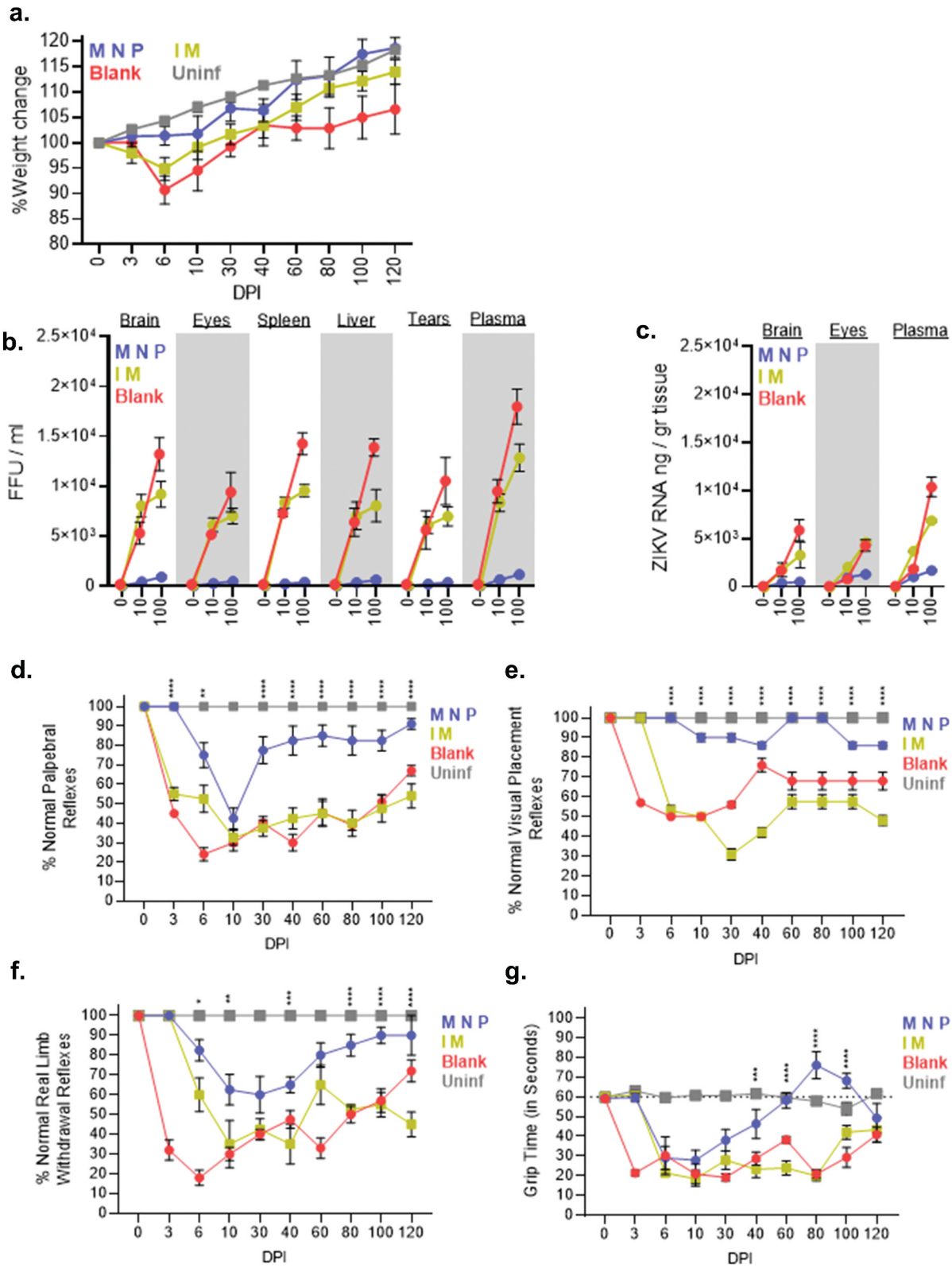

Figure 3. Cutaneous vaccination reduced viral burden and protected against pathogenic weight loss and neuro-ocular symptoms. (a) Body weight changes were monitored for 120 DPI (N = 10 for all timepoints). (b) Replication competent viral load among systemic organs, immune privileged tissues, and bodily fluids was determined by infectious co-culture (c) at 0, 10, and 100 DPI. (C) Total ZIKV genomic RNA was quantified by qRT-PCR at 0, 10, and 100 DPI (D) (Two-way ANOVA with Sidak's post-hoc; N = 5). Ocular clinical scores were determined via palpebral (d) and visual placement (e) reflex tests. (Two-way ANOVA with Sidak's post-hoc; N = 10). Motor/neural clinical scores were evaluated by rear-limb withdrawal reflex tests (f) and by grip time tests (g). The horizontal line in panel G denotes the average time a normal mouse should be able to endure test conditions. (Two-way ANOVA with Sidak's post-hoc; N = 10). For all panels, * is $p < .05$, ** is $p < .01$, *** is $p < .001$, and **** is $p < .0001$. *P* values represent the comparative differences between IM and MNP groups. Error bars represent standard deviation for all panels.

organization, and a distinct abundance of infiltrating leukocytes in the apical lumen. MNP mice showed mild hyperplasia of corneal epithelia and infiltrating leukocytes in the stroma while controls lacked these pathological features (Figure 4a, left column). Within the retinas, IM and blank vaccination mice had scleral hyperplasia, edema and subsequent degeneration of the inner and outer nuclear layers, as denoted by increases in total neural nuclei present. Additionally, ganglionic cell layers among IM recipients showed a distinct bifurcation with intense hyperplasia, potentially indicating vascular angiogenesis. In contrast, MNP retinal layers appeared normal with mild edema of RPE and limited scleral inflammation (Figure 4a, right-column).

At 100 DPI, the pathology observed in IM and blank vaccination mice was similar to 10 DPI with increased numbers of leukocytes in the stroma, loss of cellular organization among cuboidal epithelia, and warping of Descemet's and Bowman's layers. MNP corneas demonstrated edema and hyperplasia of cuboidal epithelia (Figure 4b, left column). Retinal layers of IM recipients had visible hyperplasia within the ganglionic layers, and hydropic degeneration of RPE, choroid, and sclera layers, and leukocytes in the tissue posterior to the sclera which were absent in uninfected controls. In contrast, MNP ganglionic, nuclear, and plexiform layers appeared normal, while RPE and sclera exhibited mild edema and inflammation (Figure 4b, right-column).

To assess ZIKV tropism within various tissues of the eye, we performed 4G2 immunohistochemistry on whole eyes. 4G2-positive foci detected in cornea, RPE, and lacrimal glands were enumerated 10 and 100 DPI. MNP recipients demonstrated low levels of infectivity at both time points, with a decrease from 6.5% to 2.8% between 10 and 100 DPI (Figure 4c, SFIG3 A and B). IM vaccinated mice demonstrated 4.6-times higher viral infectivity 10 DPI, and 8.8-times greater infectivity at 100 DPI compared to MNP groups, with an upward trend between early and late time-points (all $p < .0001$) (Figure 4c,d). TUNEL staining was performed in the optic tract to assess cell death 10 and 100 DPI (SFigure 3C and D). Cornea and retina were TUNEL-positive, with corneal epithelium demonstrating abundant foci in all groups. Cell death was evident at early and late time-points among all groups. MNP vaccination showed no changes in cell death at both time-points, with 2.6 to 2.1-fold higher cell death at 10 and 100 DPI, respectively, when compared to uninfected animals. IM recipients demonstrated 4.6- and 8.8-fold greater cell death compared to uninfected and blank vaccinated mice at the same time-points, doubling the rate of cell death. Importantly, IM vaccinees showed 1.7-fold greater cell death levels at 10 DPI, and 4.2-fold more 100 DPI compared to MNP (all $p < .0001$) (Figure 4e,f).

Transcriptional analysis revealed that MNP vaccination limited expression of proinflammatory cytokines after infection, with 22-times greater transcription of *IL-1β* compared to uninfected animals, whereas IM vaccination resulted in 123-times higher expression ($p = .0004$) (Figure 7g). Similarly, *TNF-α* transcription was increased 32.5-fold in MNP and 293 -fold in IM vaccinated mice ($p < .0001$). *COX2* expression was 7.3-fold lower in the eyes of the infected MNP indicating lower inflammation; IM vaccination did not alter *COX2* expression compared to MNP ($p < .001$) (Figure 4g). MMPs displayed a similar trend, where in the MNP group *MMP2* expression was 35.7-fold greater than uninfected/blank vaccinated controls, and in the IM group expression was 1,138.4-fold greater than in uninfected mice. Additionally, there was a 31.9-fold difference between IM and MNP immunized groups ($p = .006$) (Figure 4g). Finally, the MNP vaccine recipients showed an increase of 40.2- and 6.5-fold in transcription of anti-inflammatory cytokine, *IL-10* and *SOCS3*, respectively, compared to uninfected/blank vaccinated animals, while IM vaccine recipients demonstrated an increase of 442- and 17-fold compared to uninfected mice. Comparatively, MNP animals exhibited 11-fold less transcription of *IL-10* compared to IM groups, and 2.6-fold less transcription of *SOCS3* ($p = .0001$) (Figure 4g). Lower expression of anti-inflammatory proteins may point to resolution of ocular infection within MNP groups, while elevated transcription of *IL-10* and *SOCS3* correlates with H&E findings of pathogenic neovascularization. Taken together, our immunofluorescence, H&E, and transcriptional data demonstrate that weakly neutralizing antibodies correlated with intraocular pathology and fail to protect animals from ocular infectivity, persistent ocular inflammation and pronounced cell death.

MNP vaccination protected against ZIKV-induced demyelination and chronic neuroinflammation

Immunocompetent mice infected with PRVABC59 demonstrated neurological and ocular symptomatology that correlated strongly with viral burden. Viral burden was reduced by MNP vaccination, reducing severity of symptoms and improving overall convalescence and recovery. To further evaluate the impact of vaccine-induced antibodies on neuro-ocular pathology, we quantified hippocampal and cortical myelin levels using fluorescent microscopy, and determined neuro-inflammatory transcriptional responses using qRT-PCR.

Myelination of neural axons allows for electrical conduction and intracellular signaling. Within the CNS, the two most common forms of myelin are Myelin-basic protein and myelin proteolipid protein, and both are regulated by vimentin.[65] One hundred days after infection, both hippocampal and cortical regions of the MNP group's brains demonstrated that only 1.5% of cells were infected (Figure 5a). In comparison, the IM group showed identical infection levels in both regions of the brain, although they were 16-fold greater compared to MNP recipients (both $p < .0001$) (Figure 5a; SFIG4). MBP expression after MNP vaccination in both hippocampus and cortex appeared to be unaffected by infection, as fluorescence was indistinguishable from uninfected animals. IM recipients, however, exhibited 3- and 2.1-fold less MBP expression in hippocampus and cortex, respectively, when compared to both uninfected and MNP vaccinated animals (both $p < .0001$) (Figure 5b,c; SFIG4A). Both mPLP and Vim expression showed similar patterns, where MNP recipients demonstrated levels similar to uninfected and blank vaccinated animals. mPLP expression was 3.2- and 2.7-fold lower in the hippocampus and cortex, respectively, of the IM group, when compared to uninfected animals; and 4.1- and 2.2-fold lower when compared to MNP recipients (mPLP $p < .0001$ and

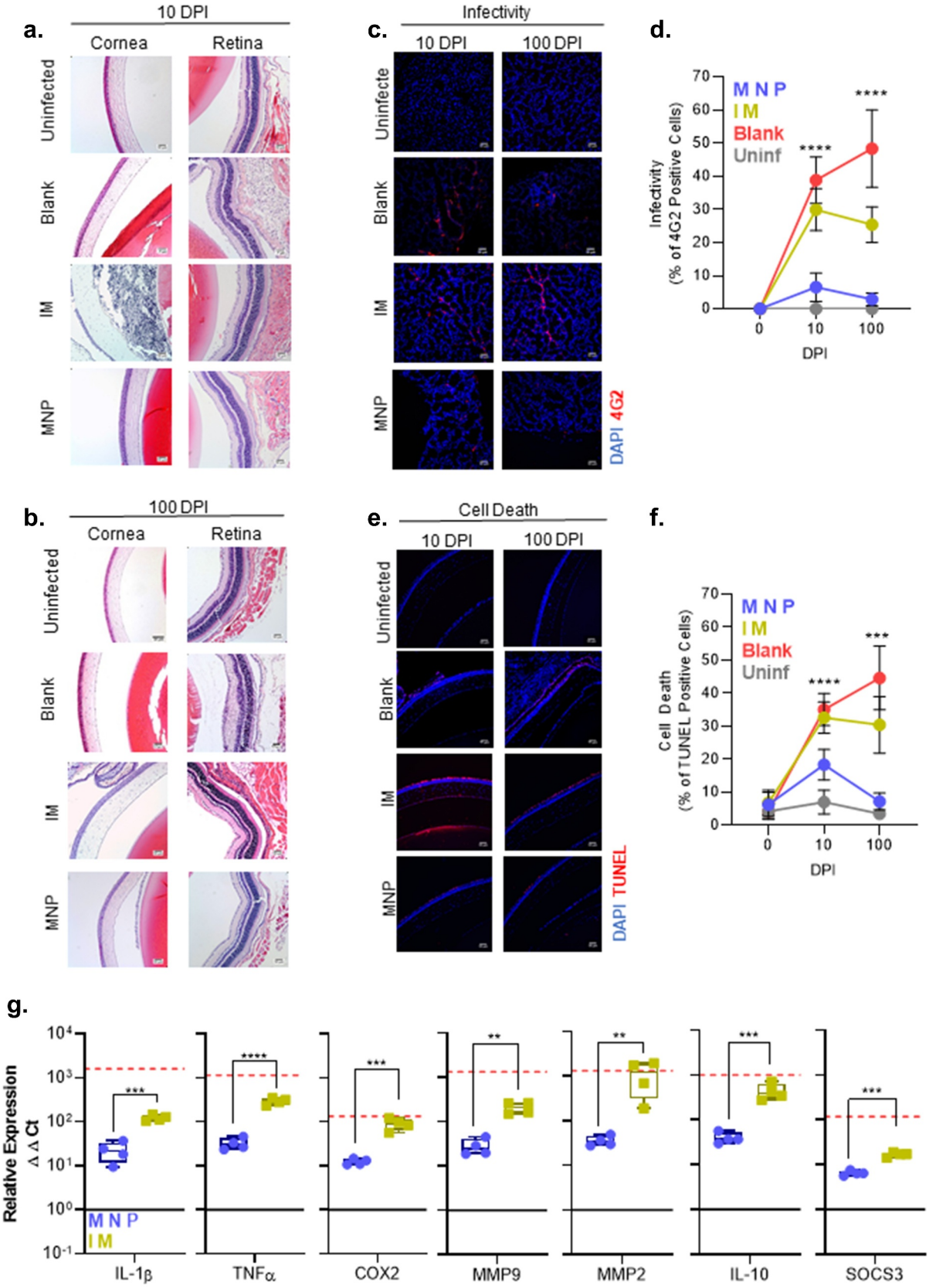

Figure 4. Low-quality antibodies triggered acute ocular pathology, increased ocular infectivity, and elevated cell death persisting up to 100 DPI. (a,b) Eyes from infected and uninfected mice were harvested 10 (a) and 100 (b) DPI for H&E and immunofluorescent staining. H&E images of corneal and retinal layers were taken at 20x to assess pathology. (c,d) ZIKV infectivity was determined by immunofluorescent staining for flavivirus antigens. The number antigen foci relative to the number of total cells in the field was calculated for both time points (Two-way ANOVA with Sidak's post-hoc; N = 10). (e,f) Similarly, TUNEL staining for cell death was performed at 10 and 100 DPI. Foci were quantified to assess infection-induced cell death (Two-way ANOVA with Sidak's post-hoc; N = 10). (g) qRT-PCR on pro-inflammatory proteins, pain mediators, MMPs, and anti-inflammatory proteins among infected brains were normalized to GAPDH and then to expression levels of uninfected controls using the ΔΔCt method. (Two-way ANOVA with Sidak's post-hoc; N = 5) Red dashed lines indicate relative expression levels detected in infected mice that received blank vaccinations. For all panels, * is $p < .05$, ** is $p < .01$, *** is $p < .001$, and **** is $p < .0001$. Error bars in all panels denote standard deviation.

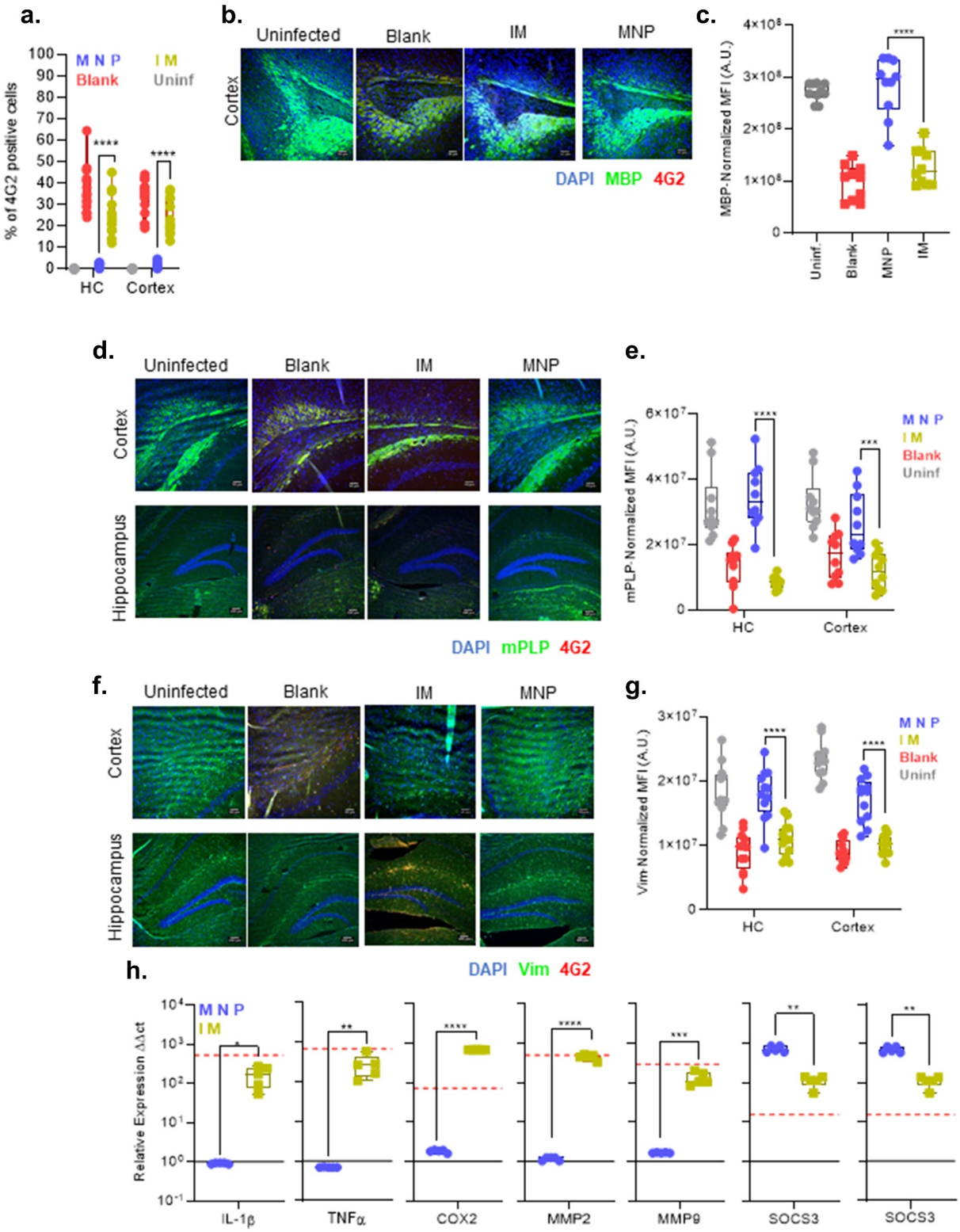

Figure 5. Low-quality antibodies elevated infection, lower myelin expression, and chronically stimulate pro-inflammatory cytokine expression. (a) Infectivity was determined by analyzing the number of 4G2 positive cells relative to the number of total cells in the field (Two-way ANOVA with Sidak's post-hoc; N = 14). (b,c) MBP expression was quantified in mid-brain cortex and hippocampus regions of infected mice (b), and was normalized to background using the CTCF method and was enumerated as normalized MFI (c; One-way ANOVA with Sidak's post-hoc analysis; N = 8). (d,e) mPLP expression was similarly quantified in mid-brain cortex (d) and hippocampus (e) regions of infected mice and was normalized to background (Two-way ANOVA with Sidak's post-hoc analysis; N = 10). (f,g) Vim expression was quantified in mid-brain cortex and hippocampus regions of infected mice using the CTCF method (f) and was normalized to background (g; Two-way ANOVA with Sidak's post-hoc analysis; N = 12). (h) qRT-PCR on pro-inflammatory proteins, pain mediators, MMPs, and anti-inflammatory proteins among infected brains were normalized to GAPDH and then to expression levels of uninfected controls using the ΔΔCt method. (Two-way ANOVA with Sidak's post-hoc; N = 5). Red dashed lines indicate relative expression levels detected among infected mice that received blank vaccination controls. For all panels, * is $p < .05$, ** is $p < .01$, *** is $p < .001$, and **** is $p < .0001$. Error bars in all panels denote standard deviation.

p = .0006; Vim both p < .0001) (Figure 5d,e). Vim expression was 1.7- and 2.3-fold lower in the hippocampus and cortex of IM vaccinated mice when compared to uninfected animals; and 1.6- and 1.7-fold lower when compared to MNP recipients (Figure 5f,g; SFIG4).

Transcriptional analysis of the inflammatory mediators in the brain revealed no change of proinflammatory *IL-1β* or *TNF-α* expression post-infection in the MNP group, comparable to uninfected controls. Infected IM vaccinees however, showed 166- and 281-fold greater transcription, respectively, compared to uninfected animals (p = .0462 and p = .0012) (Figure 5h). Pain mediator and proinflammatory stimulant, *COX2*, showed 1.8-fold greater expression among MNP mice and 678-fold higher expression in IM vaccine recipients (p < .0001) (Figure 5h). Matrix metalloproteinases (MMPs) demonstrated a trend similar to the proinflammatory cytokines, where MNP immunized animals showed transcription levels comparable to uninfected animals, while the IM immunized group demonstrated 477- and 133-fold greater transcription relative to blank vaccinated and uninfected mice for *MMP2* and *MMP9* respectively (p < .0001 and p = .0005) (Figure 5h). Finally, the levels of anti-inflammatory cytokines *IL-10* and *SOCS3* were significantly upregulated among MNP brains, with 838- and 714-fold greater levels than uninfected animals. IM immunized mice also showed elevated anti-inflammatory transcription, with 53- and 112-fold greater expression of *IL-10* and *SOCS3* compared to uninfected animals, but these levels were significantly less than MNP mice (p < .001 and p = .002) (Figure 5h). Collectively, these data demonstrate that highly specific antibodies abrogated demyelination observed during ZIKV infection and limit the chronic neuro-inflammatory response.

MNP antibodies demonstrate greater breadth of neutralization, less ADE, and are less auto-reactive

As GBS is primarily mediated by auto-reactive antibodies, we next determined if the observed reduction in neuro-ocular pathology following MNP vaccination correlated with antibody neutralization, ADE, and auto-reactivity to ganglioside residues. After infectious challenge, vaccination groups demonstrated a plateau of antibody concentrations, regardless of IgG subtypes, that endured up to 120 DPI (Figure 6a–c).

Antibodies from both vaccination groups, sampled 100 DPI, were evaluated for their ability to neutralize 3 strains of ZIKV and each of 4 DENV serotypes (Figure 7). Neutralization of the homologous strain showed a titer of 11,815 for the MNP group, and a titer of 3,265 for the IM group, a 3.6-fold difference (Figure 7a). For ZIKV-FLR, MNP-induced antibodies had a titer of 1,915 and IM-induced antibodies had a titer of 81, a 23.6-fold difference (Fig 7Bi and ii). Neutralization of MR766 showed titers of 26,887 and 3,313 for the MNP and IM vaccinated mice respectively, an 8.1-fold difference (Fig 7Bii). Among DENV strains, MNP-raised antibodies reached 21,818, 1,702, 9,219, and 30 VN titers for DENV-1 through −4 respectively. IM-induced antibodies had neutralizing titers of 208, 397, 185, and 2 for the same strains. Thus, MNP antibody neutralization titers were 104.9-, 4.3-, 50.2-, and 15-fold greater than IM titers for DENV-1, DENV-2, DENV-3, and DENV-4, respectively (SFIG 5Aiii-vi) (all neutralization titers are listed in Sup Figure 5A).

The capability of vaccination-induced antibodies to enhance homologous and heterologous flavivirus infection were also quantified for both maximum infectivity and the associated endpoint titers (Sup Figure 5B). Ideal vaccine candidates would minimize ZIKV infection by ADE, regardless of strain, and demonstrate limited DENV reactivity. Co-incubation of ZIKV or DENV strains and U937 cells resulted in no detected infection. MNP-induced antibodies limited ADE infection of the permissive U937 cells. Following antibody co-incubation with PRVABC59, a maximum of 5% of the 10,000 cells assayed were positive for ZIKV infection (Figure 7A). The same antibodies generated a maximum of 10% and 18% of all infected cells when the FLR or MR766 strains were used (Figure 8b–i and ii). Among DENV serotypes, MNP-induced antibodies resulted in a maximum of 22% of all cells labeled positive for DENV-1 infection, 36% of cells were positive for DENV-2, 24% were positive for DENV-3, and 19% were positive for DENV-4 (SFIG 6Aiii-vi). When infectious virus was co-incubated with antibodies generated by IM vaccination, the frequency of cells positive for infection increased dramatically. The IM group showed a maximum of 84.6% of all cells infected with PRVABC59 (Figure 8a), while FLR and MR766 demonstrated a maximum of 70% and 90% cell infectivity, respectively (Figure 8b–i,ii). IM-vaccination antibodies resulted in 72% of cells infected with DENV-1, 54% infected with DENV-2, 41% infected with DENV-3, and 86% infected with DENV-4 (Fig 8Biii – vi).

Collectively, these data demonstrate that antibodies generated via MNP vaccination were of greater immunological quality than those generated by IM, as evidenced by the reduced viral burden and limitation of clinical symptoms and tissue pathology after infection.

To correlate observed neuro-ocular pathology with GBS-like autoantibodies, we determined the relative concentrations of anti-ganglioside autoantibodies generated by MNP and IM vaccinations. Thus, we quantified the total amount of IgG that bound to GD1a, GD1b, and GT1a gangliosides (Figure 9a–c). Each of these correlates with a specific variety of GBS. GD1a reactive IgG correlates with acute motor axonal neuropathy; GD1b corresponds to a sensory ataxic variant; GT1a is connected to Miller-Fisher Syndrome, a variant of GBS affecting the eyes.[66] To understand what quantity of these antibodies are auto-reactive, we took the percentage of each ganglioside concentration as a proportion to the total ZIKV-specific IgG. In the MNP vaccinated group, 12% of all antibodies were GD1a reactive prior to infectious challenge and never exceeded 15% after challenge. Prior to challenge, 16% of IM induced antibodies were GD1a-reactive, and after challenge, a maximum of 25.1% of all antibodies showed autoreactivity 60 DPI (Figure 9a). For all time-points observed, MNP antibodies were significantly less reactive to GD1a than those induced by IM vaccination (p = .008 at 0 DPI, all other p < .0001). Thirteen percent of MNP antibodies prior to vaccination were reactive to GD1b and reached a maximum of 19% 10 DPI (Figure 9b). Twenty-two percent of IM vaccination-induced antibodies were reactive to GD1b prior to challenge, and reached

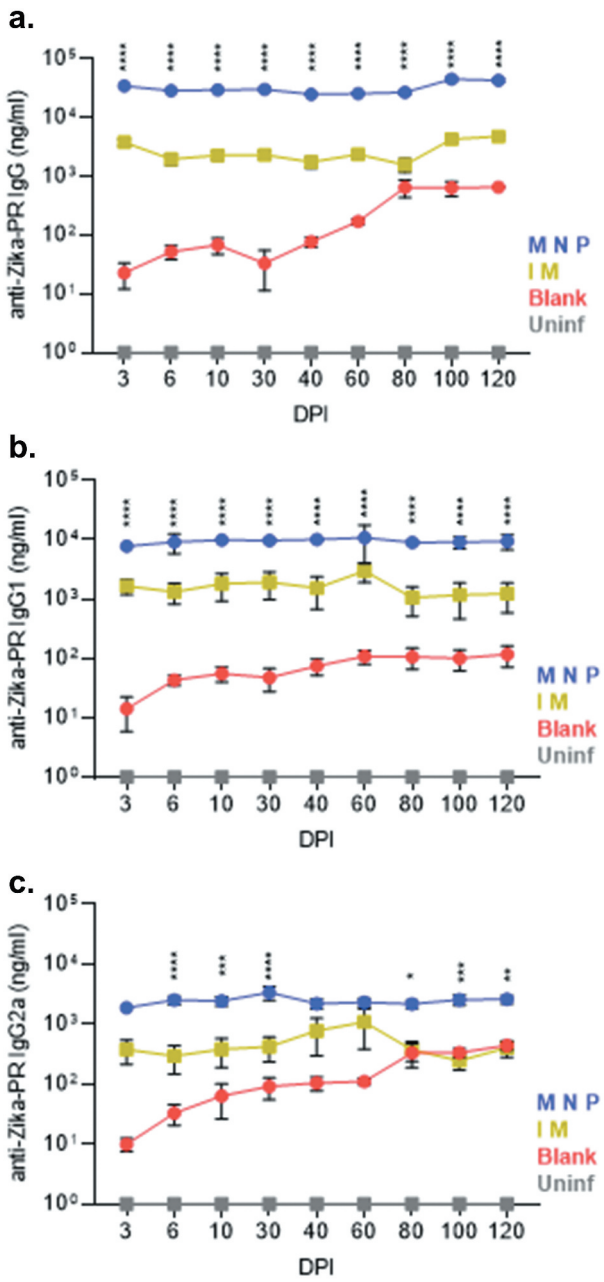

Figure 6. Antibodies generated by MNP vaccination remain elevated after infection challenge. ZIKV-specific antibody kinetics were quantified up to 120 DPI for IgG total (a), IgG1 (b), IgG2a (c). Time-points were analyzed using Two-way ANOVA with Sidak's post-hoc correction (N = 10). For all panels, * is $p < .05$, ** is $p < .01$, *** is $p < .001$, and **** is $p < .0001$. Error bars in all panels denote standard deviation.

a maximum of 25% after challenge 10 DPI. Again, for all time-points observed, MNP antibodies were significantly less reactive to GD1b than those induced by IM vaccination ($p = .001$ at 10 DPI, all other $p < .0001$). Twelve percent of MNP antibodies prior to vaccination were reactive to GT1a and reached a maximum of 38% 60 DPI (Figure 9c). Sixteen percent of IM vaccination-induced antibodies were reactive to GT1a prior to challenge and reached a maximum of 25% after challenge 10 DPI. Similarly, MNP antibodies were significantly less reactive to GD1b than those induced by IM vaccination throughout the observation period ($p = .001$ at 10 DPI, all other $p < .0001$).

Discussion

ZIKV has remained as an international health concern since its re-appearance in 2015. It is increasingly apparent that the impact of ZIKV extends beyond microcephaly, as children born to infected mothers continually present new neurological and ocular clinical manifestations.[67,68] As a result, there has been substantial interest in understanding the mechanisms behind ZIKV invasion and persistence in immune-privileged tissues, as well as a sustained interest in viable vaccine candidates. Ocular and neurological pathology observed in humans has successfully been recapitulated in both WT and immunocompromised murine models, but has not been utilized to evaluate vaccine efficacy despite the potential correlation between GBS and ZIKV-induced long- term pathology. Here, we demonstrated that immunocompetent BALB/c mice developed unique ocular and neuro-motor pathology as a result of ZIKV infection, and that this pathology can be abrogated with cutaneous immunization using MNPs encapsulating unadjuvanted whole, particle vaccine.

Importantly, we demonstrate that this route of vaccination can generate broadly neutralizing antibodies against multiple strains of ZIKV and DENV, while limiting antibody-mediated infection among non-permissive Fcγ-R bearing macrophages. We also show that the same unadjuvanted vaccine delivered intramuscularly induces weak and short-lived cellular responses, which ultimately result in broadly cross-reactive antibodies with limited neutralizing activity and elevated ADE capabilities compared to MNP vaccination. IM vaccination induced antibodies that enhanced ADE -similarly to infected controls that received blank vaccinations; further supporting the hypothesis that antibodies generated by an IM delivered unadjuvanted ZIKV were of low immunological quality. This hypothesis was validated by our avidity analysis showing that antibodies in the IM vaccinated cohort had lower avidity than the MNP cohort. Collectively, this data indicates the necessity of adjuvants in conventional vaccination routes to stimulate more robust cellular and humoral responses. Indeed, recent studies point to the importance of a strong $CD4^+$ and $CD8^+$ T cell responses, where $CD4^+$ T cells are critical in systemic clearance of ZIKV and prevent ZIKV neuroinvasion,[44] while $CD8^+$ T cells and T cell-derived IFN-γ are essential to protecting microglia during ZIKV infection.[13]

The observed neuroinflammation and neuro-ocular pathology was consistent with published data showing how flavivirus infections culminate in chronic neurological inflammation that directly contributes to lethal motor/cognitive diseases, such as GBS.[69] MNP vaccination conferred protection of ocular and brain micro-environments against viral infection, as shown by a reduction of *COX2, TNF-α*, and *IL-1β* transcription, which was consistently lower than IM vaccination counterparts. These three pro-inflammatory markers created a positive feedback loop in the context of microglial secretion, where IL-1β and TNF-α secretion by glial cells is stimulated by COX2,[70] and paracrine or autocrine IL-1β signaling through NF-kB signaling.[71,72] Similar to the reduction of pro-inflammatory transcription, MNP vaccination resulted in lower transcription of *MMP2* and *MMP9* than IM vaccination after infectious challenge. MMPs are

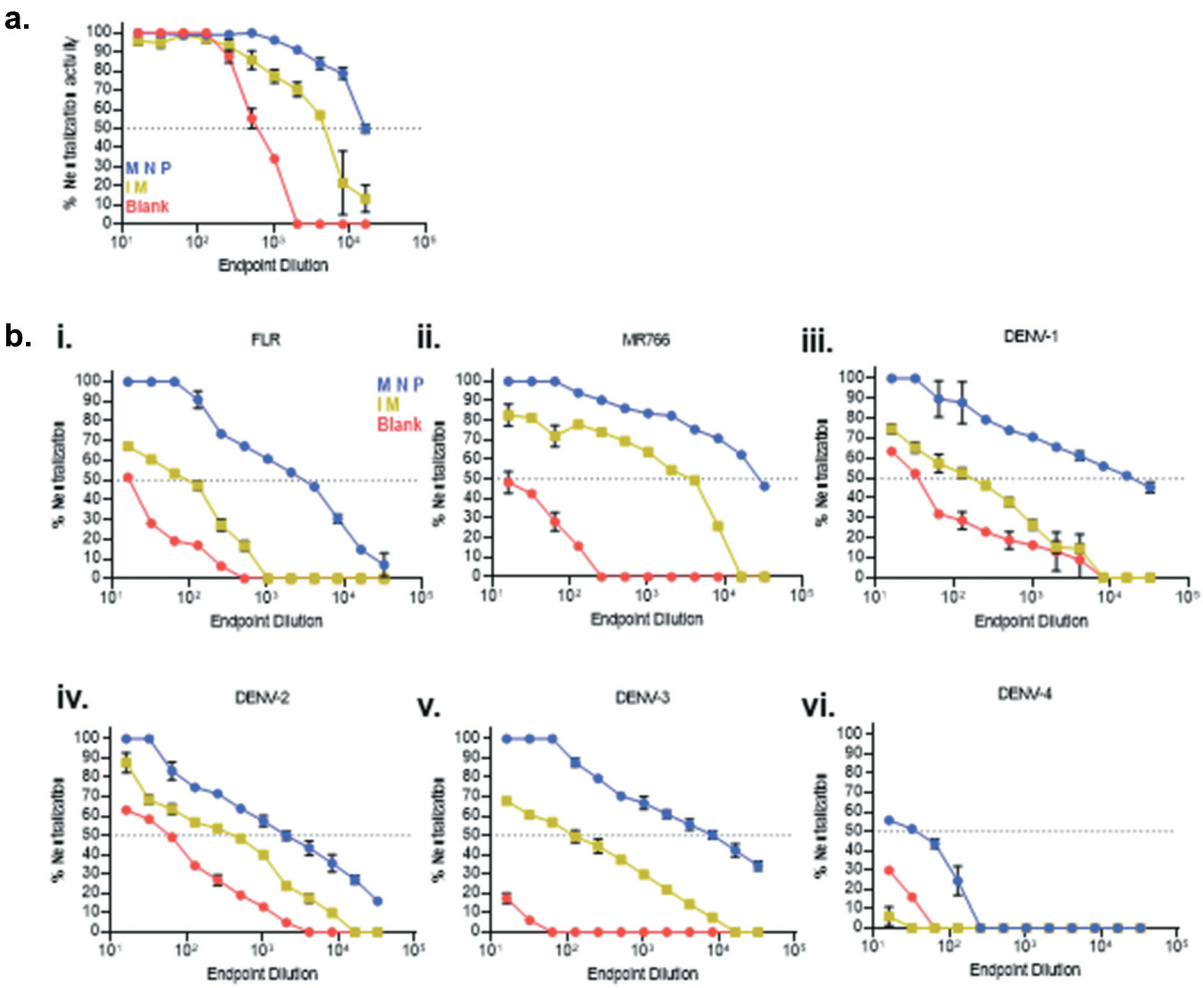

Figure 7. IM-induced antibodies demonstrated lower neutralizing activity than those generated by MNP. (a) Endpoint IC_{50} antibody dilutions were determined for MNP and IM vaccinated animals 100 DPI using the PRVABC59 strain of ZIKV. (b) Neutralization was also determined using the (i) FLR, and (ii) MR766 strains of ZIKV in addition to (iii) DENV1/Hawaii/1944, (iv) DENV2/16681/Thailand/1964, (v) DENV3/H87/Philippines/1956, and (vi) DENV4/UNC4019/Colombia/2006. The dotted line denotes 50% neutralization. Error bars represent standard deviation for all panels.

endopeptidases with vital functions such as neural network remodeling, tissue destruction and restructure, and BBB integrity regulation.[73,74] Thus, infection that induces increased permeability of the BBB via elevated transcription of *MMP2* and *MMP9* corresponds to increased inflammatory leukocyte trafficking into the brain.[75,76] For both brain and eyes, the relative transcription levels of *COX2, IL-1β, TNF-α, MMP2*, and *MMP9* among ZIKV-infected MNP vaccinated animals never exceeded a 2-fold difference and were statistically similar to blank vaccinated control mice, indicating a robust protection of these tissues using the MNP vaccination platform. Conversely, IM vaccination-induced transcription levels of these same markers were at least 100-fold higher than MNP vaccinations, but were not statistically different from animals that received blank vaccinations, indicating the cellular and humoral responses generated by IM immunizations were not protective in immune-privileged compartments.

Even though the eye and brain are intricately linked immune-privileged compartments, our data demonstrated that vaccination differentially impacted the anti-inflammatory responses within these tissues. Anti-inflammatory proteins IL-10 and SOCS3 form a unique pathway, whereby following stimulation with TNF-α and IL-6 by local resident and infiltrating immune cells producing IL-10.[77] The latter then stimulates SOCS3 production, and both work in concert to block intracellular signaling of IL-6 and IL-23, to prevent STAT3 phosphorylation and directly influence ocular T cell repertoire.[78] Infected brain tissues showed that MNP elevated both IL-10 and SOCS3 more than IM counterparts. As IL-10 has demonstrated the ability to protect astrocytes from excessive inflammation,[79,80] our data demonstrated that MNP vaccination conferred protection against long-term neuro-inflammation in a manner that IM vaccination did not. Within the eye, IL-10 and SOCS3 have a counter-intuitive mechanism. Previous studies have demonstrated that high intraocular concentrations of these anti-inflammatory cytokines could stimulate angiogenesis via Müller-cell mediated neovascularization.[81] Of particular note, IM vaccination appeared to exacerbate ocular pathology 10 DPI, with intense infiltration of monocytes and granulocytes into both the vitreous and apical lumen. Leukocyte infiltration occurred alongside

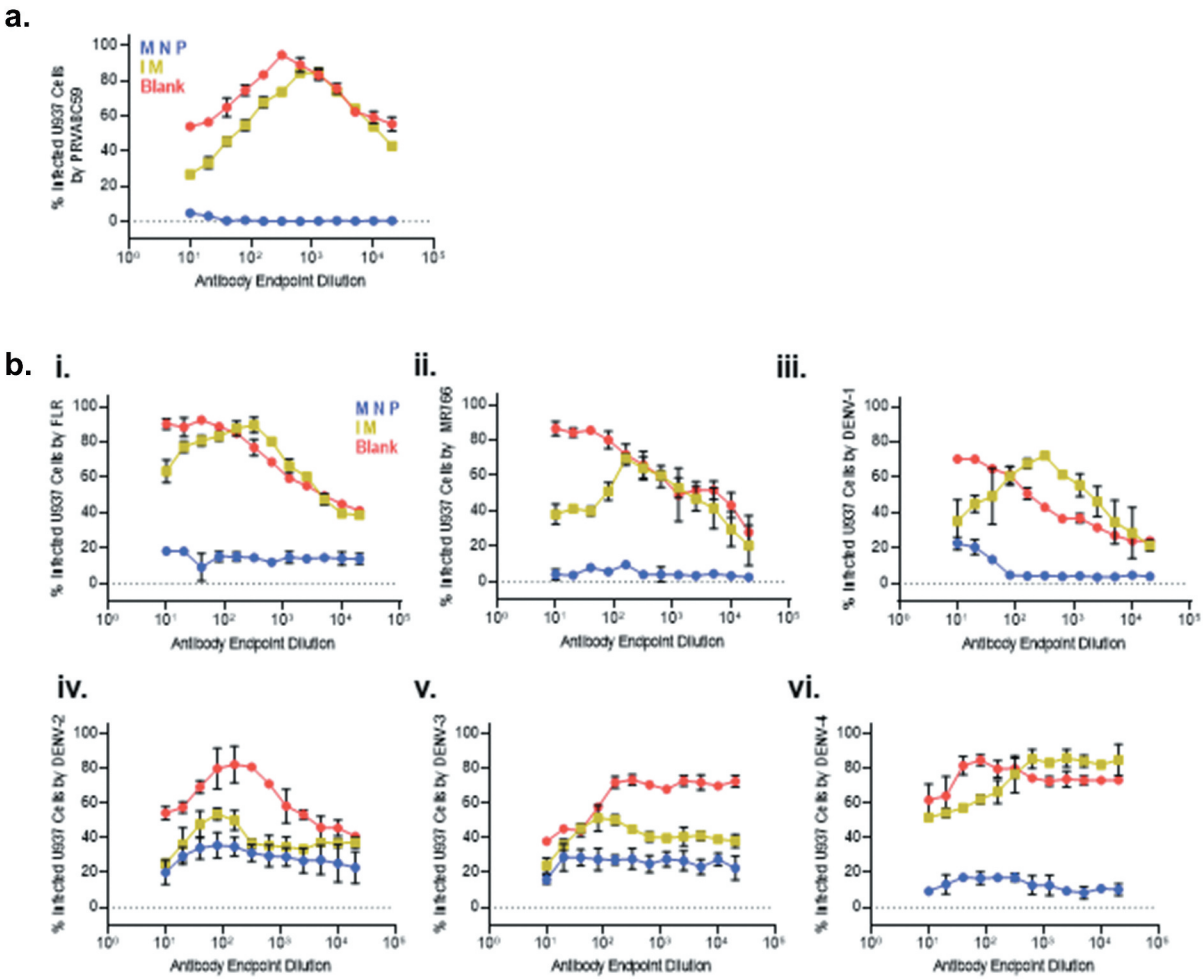

Figure 8. IM-induced antibodies enhanced infection among non-permissive FcγR-bearing cells, whereas MNP antibodies limit ADE. (a) ADE capacity was measured for MNP and IM vaccinated antibodies 100 DPI for the PRVABC59 strain of ZIVK. (b) ADE was also determined using the (i) FLR, and (ii) MR766 strains of ZIKV in addition to (iii) DENV1/Hawaii/1944, (iv) DENV2/16681/Thailand/1964, (v) DENV3/H87/Philippines/1956, and (vi) DENV4/UNC4019/Colombia/2006. The dotted line denotes background fluorescence determined by cells combined with virus but no antibodies. Error bars represent standard deviation for all panels.

a bifurcation of the ganglionic cell layers of infected retinas, demonstrating ocular pathology was not specific to a single tissue layer of the eye.

Our study is the first to report on MNP vaccination used against ZIKV, and that autoreactive antibodies to GD1a, GD1b, and GT1a gangliosides are increased following unadjuvanted IM vaccination, which contributed to myelin degradation in immunocompetent BALB/c mice following infection.[82] GBS has been correlated with antibody cross-reactivity to host gangliosides in other flaviviruses,[83,84] but is rarely studied as a consequence of flavivirus vaccination. We observed that 25–75% of all PRVABC59-specfic antibodies generated by ZIKV infection that were specific PRVABC59 were autoreactive, and that MNP vaccination lower this proportion to 14–19%, while IM vaccination had 25–40% of autoreactive antibodies. Gangliosides are vital to synaptic transmissions, intercellular adhesion and communication, equilibrium, immune signaling, and nervous system and motor/neural network maintenance.[85] Anti-ganglioside antibodies have been previously shown to lead to the absence or fragmentation of MBP, myelin PLP, and vimentin, all contributing to persistent neuroinflammation within the brain by releasing damage associated molecular patterns (DAMPs)[86]. Myelin or myelin-debris signals in macrophages via complement/opsonization or phagocytosis and facilitates M1 (macrophage type-1) polarization and proinflammatory secretion[86]. This M1 microglia polarization is associated with prolonged secretion of TNF-α at high levels and can lead to permanent neural degeneration. This observation, correlated with our transcriptional data of blank vaccinated and IM vaccinated animals demonstrating chronic neuroinflammation and demyelination.

Our study points to the need for a more comprehensive, systems biology approach to understand how antibodies influence long-term neurological pathogenesis of flaviviruses. Our data suggests that low specificity of ZIKV antibodies may initiate a demyelination cascade that ultimately resultes in chronic neuroinflammation and persistent neuro/ocular impairments. This adverse pathology can be circumvented by novel vaccination approaches that generate highly specific, strongly neutralizing antibodies despite the absence of an adjuvant. These antibodies limit infection of Fcγ-R bearing

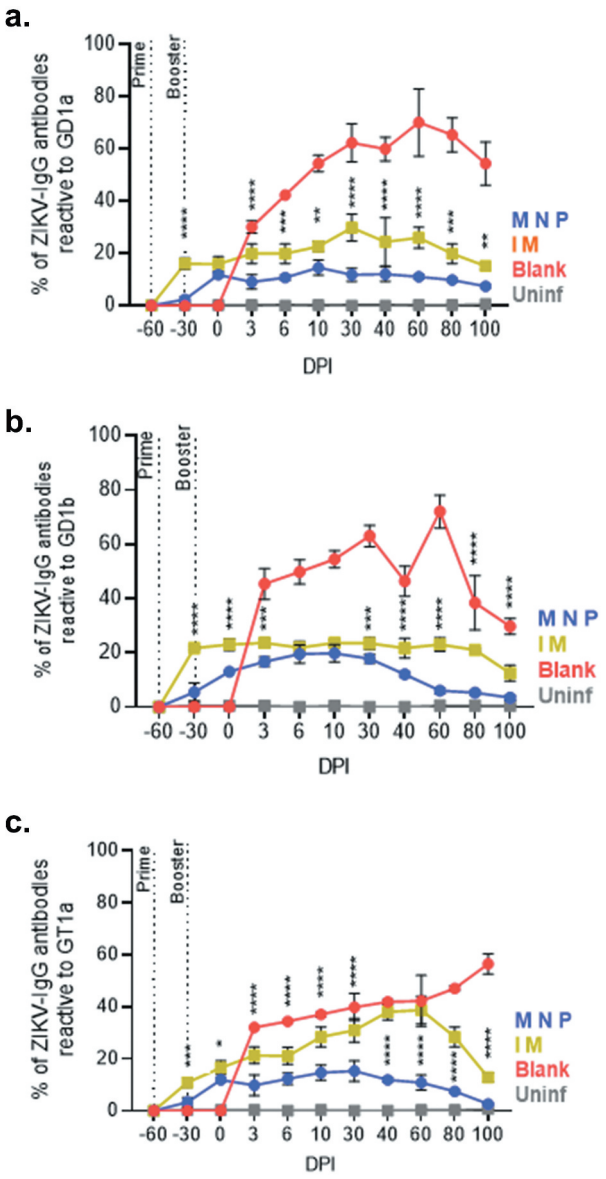

Figure 9. Antibodies generated by MNP vaccination were less auto-reactive to gangliosides. ZIKV-specific antibodies were evaluated for autoreactivity to host gangliosides GD1a (a), GD1b (b), and GT1a (c). (Two-way ANOVA with Sidak's post-hoc; N = 5). For all panels, * is $p < .05$, ** is $p < .01$, *** is $p < .001$, and **** is $p < .0001$. Error bars in all panels denote standard deviation.

macrophages via ADE mechanisms and demonstrated limited autoreactivity to GBS-associated residues. Importantly, we demonstrated here that immunocompetent animals can serve as models for long-term vaccination studies, and denote highlight that the need for adjuvants depends on the antigen administration route. Our findings point to the need of exploring alternative vaccination platforms and imposing stringent qualifications for ZIKV vaccine candidates: vaccines must that would confer breadth and longevity of protection while minimizing the risk of autoimmunity and ADE. Future studies should include investigation of demyelination sequelae after passive transfer of ZIKV-induced antibodies, and the putative role of maternal antibodies on vertical transmission. Additionally, future studies duplicating this work in C57BL/6 mice will determine if similar pathology can be observed in a Th1-skewed background.

Ethics statement

Emory University Division of Animal Resources veterinary staff ascertained welfare of animals in addition to research scientists. DAR staff performed regular care and wellness assessments. Animal work was conducted according to Emory University Institutional Animal Care and Use Committee (IACUC) guidelines according to an approved protocol (DAR2002950-122617BN) and in accordance with the United States federal Animal Welfare Act (PL 89–544) and subsequent amendments. Emory University is registered with the United States Department of Agriculture (57-R-003) and has filed an Assurance of Compliance statement with the Office of Laboratory Animal Welfare of the National Institutes of Health (D16-00113). Emory University has been fully and continuously accredited by AAALAC International since 1992 (Unit 000781). The Georgia Fee-Exempt Wild Animal Permit Customer Number for animals maintained by the Division of Animal Resources is 22257.

Acknowledgments

We thank Dr. Sharon Isern' Dr. Scott Michael, and Lauren Paul for providing the ZIKV PRVABC59 strain for propagation.

We thank Dr. Micah Chrenek, Dr. Hans Grossniklaus, and Dr. John Nickerson from Emory Ophthalmology Clinic for their advice on optic histology and staining.

We thank Dr. Eugenia Scountzou and Dr. Nikolaos Papaioannou for their expertise in veterinary ophthalmology and for detailed assistance in evaluating animal ocular pathology.

We thank Dr. Kiran Gill at Emory Vaccine Center core facility for her expert advice with flow cytometry.

We thank Vidisha Singh and Aaron Scanlon for assistance running qRT-PCR experiments.

Funding

This work was supported by NIAID and CEIRS [HHSN272201400004C NIAID].

ORCID

Ioanna Skountzou http://orcid.org/0000-0002-6429-244X

Author contribution

J.T.B., N.L., I.S., E.S. Project conceptualization and experimental design

J.T.B., L.K.M., E.S.E., D.S., N.L., O.Q.A., E.Q.L., I.S.: Execution of experiments

E.S. and N.P. Assessment of ocular pathology

J.T.B, N.L., D.S., and I.S. Data analysis.

A.R.: Development and fabrication of MNP

J.T.B., D.S. and I.S. Manuscript preparation

M.R.P.: Overseeing ZVIP-MNP development

R.W.C. Manuscript feedback.

All authors read and provided feedback prior to submission

Competing financial interests

M.R.P. is an inventor of patents licensed to companies developing microneedle-based products, is a paid advisor to companies developing microneedle-based products and is a founder/shareholder of companies

developing microneedle-based products (Micron Biomedical). This potential conflict of interest has been disclosed and is managed by Georgia Tech and Emory University. J.T.B., L.K.M., E.S.E., D.S., N.L., O.Q.A., E.S., N.P., D.T.W., A.R., R.W.C., and I.S. declare that they have no conflicts of interest.

References

1. Araujo LM, Ferreira ML, Nascimento OJ. Guillain-Barre syndrome associated with the Zika virus outbreak in Brazil. Arq Neuropsiquiatr. 2016;74:253–55. doi:10.1590/0004-282X20160035.
2. Brasil P, Pereira JP, Moreira ME, Ribeiro Nogueira RM, Damasceno L, Wakimoto M, Rabello RS, Valderramos SG, Halai U-A, Salles TS, *et al.* Zika Virus Infection in pregnant women in Rio de Janeiro. N Engl J Med. 2016;375:2321–34. doi:10.1056/NEJMoa1602412.
3. da Silva IRF, Frontera JA, Bispo de Filippis AM, Nascimento O, Group R-G-ZR. Neurologic complications associated with the Zika Virus in Brazilian adults. JAMA Neurol. 2017;74:1190–98. doi:10.1001/jamaneurol.2017.1703.
4. Barzon L, Pacenti M, Franchin E, Lavezzo E, Trevisan M, Sgarabotto D, Palu G. Infection dynamics in a traveller with persistent shedding of Zika virus RNA in semen for six months after returning from Haiti to Italy, January 2016. Euro Surveill. 2016;21. doi:10.2807/1560-7917.ES.2016.21.32.30316.
5. Mansuy JM, Dutertre M, Mengelle C, Fourcade C, Marchou B, Delobel P, Izopet J, Martin-Blondel G. Zika virus: high infectious viral load in semen, a new sexually transmitted pathogen? Lancet Infect Dis. 2016;16:405. doi:10.1016/S1473-3099(16)00138-9.
6. Murray KO, Gorchakov R, Carlson AR, Berry R, Lai L, Natrajan M, Garcia MN, Correa A, Patel SM, Aagaard K, *et al.* Prolonged detection of Zika virus in Vaginal secretions and whole blood. Emerg Infect Dis. 2017;23:99–101. doi:10.3201/eid2301.161394.
7. Bandyopadhyay D, Hajra A. ZIKA virus: A new threat to the eyes. Eur J Intern Med. 2017;44:e9–e10. doi:10.1016/j.ejim.2017.05.022.
8. Prakalapakorn SG, Meaney-Delman D, Honein MA, Rasmussen SA. The eyes as a window to improved understanding of the prenatal effects of Zika virus infection. J Aapos. 2017;21:259–61. doi:10.1016/j.jaapos.2017.07.001.
9. Munoz LS, Parra B, Pardo CA; Neuroviruses Emerging in the Americas, S. Neurological implications of Zika Virus infection in adults. J Infect Dis. 2017;216:S897–S905. doi:10.1093/infdis/jix511.
10. Barbi L, Coelho AVC, Alencar LCA, Crovella S. Prevalence of Guillain-Barre syndrome among Zika virus infected cases: a systematic review and meta-analysis. Braz J Infect Dis. 2018;22:137–41. doi:10.1016/j.bjid.2018.02.005.
11. Dimachkie MM, Barohn RJ. Guillain-Barre syndrome and variants. Neurol Clin. 2013;31:491–510. doi:10.1016/j.ncl.2013.01.005.
12. Nachamkin I, Allos BM, Ho T. Campylobacter species and Guillain-Barre syndrome. Clin Microbiol Rev. 1998;11:555–67. doi:10.1128/CMR.11.3.555.
13. Garber C, Soung A, Vollmer LL, Kanmogne M, Last A, Brown J, Klein RS. T cells promote microglia-mediated synaptic elimination and cognitive dysfunction during recovery from neuropathogenic flaviviruses. Nat Neurosci. 2019;22:1276–88. doi:10.1038/s41593-019-0427-y.
14. McDonald EM, Duggal NK, Delorey MJ, Oksanish J, Ritter JM, Brault AC. Duration of seminal Zika viral RNA shedding in immunocompetent mice inoculated with Asian and African genotype viruses. Virology. 2019;535:1–10. doi:10.1016/j.virol.2019.06.010.
15. Singh PK, Guest J-M, Kanwar M, Boss J, Gao N, Juzych MS, Abrams GW, Yu F-S, Kumar A. Zika virus infects cells lining the blood-retinal barrier and causes chorioretinal atrophy in mouse eyes. JCI Insight. 2017;2:e92340. doi:10.1172/jci.insight.92340.
16. Simonin Y, Erkilic N, Damodar K, Clé M, Desmetz C, Bolloré K, Taleb M, Torriano S, Barthelemy J, Dubois G, *et al.* Zika virus induces strong inflammatory responses and impairs homeostasis and function of the human retinal pigment epithelium. EBioMedicine. 2019;39:315–31. doi:10.1016/j.ebiom.2018.12.010.
17. Pardi N, Hogan MJ, Pelc RS, Muramatsu H, Andersen H, DeMaso CR, Dowd KA, Sutherland LL, Scearce RM, Parks R, *et al.* Zika virus protection by a single low-dose nucleoside-modified mRNA vaccination. Nature. 2017;543:248–51. doi:10.1038/nature21428.
18. Shan C, Muruato AE, Nunes BTD, Luo H, Xie X, Medeiros DBA, Wakamiya M, Tesh RB, Barrett AD, Wang T, *et al.* A live-attenuated Zika virus vaccine candidate induces sterilizing immunity in mouse models. Nat Med. 2017;23:763–67. doi:10.1038/nm.4322.
19. Calvet GA, Kara EO, Giozza SP, Bôtto-Menezes CHA, Gaillard P, de Oliveira Franca RF, de Lacerda MVG, da Costa Castilho M, Brasil P, de Sequeira PC, *et al.* Study on the persistence of Zika virus (ZIKV) in body fluids of patients with ZIKV infection in Brazil. BMC Infect Dis. 2018;18:49. doi:10.1186/s12879-018-2965-4.
20. Gaudinski MR, Houser KV, Morabito KM, Hu Z, Yamshchikov G, Rothwell RS, Berkowitz N, Mendoza F, Saunders JG, Novik L, *et al.* Safety, tolerability, and immunogenicity of two Zika virus DNA vaccine candidates in healthy adults: randomised, open-label, phase 1 clinical trials. Lancet. 2018;391:552–62. doi:10.1016/S0140-6736(17)33105-7.
21. Modjarrad K, Lin L, George SL, Stephenson KE, Eckels KH, De La Barrera RA, Jarman RG, Sondergaard E, Tennant J, Ansel JL, *et al.* Preliminary aggregate safety and immunogenicity results from three trials of a purified inactivated Zika virus vaccine candidate: phase 1, randomised, double-blind, placebo-controlled clinical trials. Lancet. 2018;391:563–71. doi:10.1016/S0140-6736(17)33106-9.
22. Beaver JT, Lelutiu N, Habib R, Skountzou I. Evolution of two major zika virus lineages: implications for pathology, immune response, and vaccine development. Front Immunol. 2018;9:1640. doi:10.3389/fimmu.2018.01640.
23. Barrett ADT. Current status of Zika vaccine development: zika vaccines advance into clinical evaluation. NPJ Vaccines. 2018;3:24. doi:10.1038/s41541-018-0061-9.
24. Moffatt K, Wang Y, Raj Singh TR, Donnelly RF. Microneedles for enhanced transdermal and intraocular drug delivery. Curr Opin Pharmacol. 2017;36:14–21. doi:10.1016/j.coph.2017.07.007.
25. Nguyen TT, Park JH. Human studies with microneedles for evaluation of their efficacy and safety. Expert Opin Drug Deliv. 2018;15:235–45. doi:10.1080/17425247.2018.1410138.
26. Prausnitz MR. Engineering microneedle patches for vaccination and drug delivery to skin. Annu Rev Chem Biomol Eng. 2017;8:177–200. doi:10.1146/annurev-chembioeng-060816-101514.
27. Del Pilar Martin M, Weldon WC, Zarnitsyn VG, Koutsonanos DG, Akbari H, Skountzou I, Jacob J, Prausnitz MR, Compans RW. Local response to microneedle-based influenza immunization in the skin. MBio. 2012;3:e00012–00012. doi:10.1128/mBio.00012-12.
28. Pulit-Penaloza JA, Esser ES, Vassilieva EV, Lee JW, Taherbhai MT, Pollack BP, Prausnitz MR, Compans RW, Skountzou I. A protective role of murine langerin(+) cells in immune responses to cutaneous vaccination with microneedle patches. Sci Rep. 2014;4:6094. doi:10.1038/srep06094.
29. Sullivan SP, Koutsonanos DG, Del Pilar Martin M, Lee JW, Zarnitsyn V, Choi S-O, Murthy N, Compans RW, Skountzou I, Prausnitz MR, *et al.* Dissolving polymer microneedle patches for influenza vaccination. Nat Med. 2010;16:915–20. doi:10.1038/nm.2182.
30. Koutsonanos DG, Vassilieva EV, Stavropoulou A, Zarnitsyn VG, Esser ES, Taherbhai MT, Prausnitz MR, Compans RW, Skountzou I. Delivery of subunit influenza vaccine to skin with microneedles improves immunogenicity and long-lived protection. Sci Rep. 2012;2:357. doi:10.1038/srep00357.
31. Vassilieva EV, Wang S, Li S, Prausnitz MR, Compans RW. Skin immunization by microneedle patch overcomes statin-induced suppression of immune responses to influenza vaccine. Sci Rep. 2017;7:17855. doi:10.1038/s41598-017-18140-0.
32. Hamel R, Dejarnac O, Wichit S, Ekchariyawat P, Neyret A, Luplertlop N, Perera-Lecoin M, Surasombatpattana P,

Talignani L, Thomas F, *et al*. Biology of Zika Virus Infection in Human Skin Cells. J Virol. 2015;89:8880–96. doi:10.1128/JVI.00354-15.
33. Mackay LK, Rahimpour A, Ma JZ, Collins N, Stock AT, Hafon M-L, Vega-Ramos J, Lauzurica P, Mueller SN, Stefanovic T, *et al*. The developmental pathway for CD103(+) CD8+ tissue-resident memory T cells of skin. Nat Immunol. 2013;14:1294–301. doi:10.1038/ni.2744.
34. Nazerai L, Schøller AS, Rasmussen POS, Buus S, Stryhn A, Christensen JP, Thomsen AR. A New In Vivo Model to Study Protective Immunity to Zika Virus Infection in Mice With Intact Type I Interferon Signaling. Front Immunol. 2018;9:593. doi:10.3389/fimmu.2018.00593.
35. Coelho SVA, Neris RLS, Papa MP, Schnellrath LC, Meuren LM, Tschoeke DA, Leomil L, Verçoza BRF, Miranda M, Thompson FL, *et al*. Development of standard methods for Zika virus propagation, titration, and purification. J Virol Methods. 2017;246:65–74. doi:10.1016/j.jviromet.2017.04.011.
36. Matrosovich M, Matrosovich T, Garten W, Klenk HD. New low-viscosity overlay medium for viral plaque assays. Virol J. 2006;3:63. doi:10.1186/1743-422X-3-63.
37. Priyamvada L, Quicke KM, Hudson WH, Onlamoon N, Sewatanon J, Edupuganti S, Pattanapanyasat K, Chokephaibulkit K, Mulligan MJ, Wilson PC, *et al*. Human antibody responses after dengue virus infection are highly cross-reactive to Zika virus. Proc Natl Acad Sci U S A. 2016;113:57852–57. doi:10.1073/pnas.1607931113.
38. Garcia-Nicolas O, Braun RO, Milona P, Lewandowska M, Dijkman R, Alves MP, Summerfield A. Targeting of the Nasal Mucosa by Japanese Encephalitis Virus for Non-Vector-Borne Transmission. J Virol. 2018:92. doi:10.1128/JVI.01091-18.
39. Durbin A, Wilder-Smith A. An update on Zika vaccine developments. Expert Rev Vaccines. 2017;16:781–87. doi:10.1080/14760584.2017.1345309.
40. Abbink P, Larocca RA, De La Barrera RA, Bricault CA, Moseley ET, Boyd M, Kirilova M, Li Z, Nganga D, Nanayakkara O, *et al*. Protective efficacy of multiple vaccine platforms against Zika virus challenge in rhesus monkeys. Science. 2016;353:1129–32. doi:10.1126/science.aah6157.
41. Littauer EQ, Mills LK, Brock N, Esser ES, Romanyuk A, Pulit-Penaloza JA, Vassilieva EV, Beaver JT, Antao O, Krammer F, *et al*. Stable incorporation of GM-CSF into dissolvable microneedle patch improves skin vaccination against influenza. J Control Release. 2018;276:1–16. doi:10.1016/j.jconrel.2018.02.033.
42. Vassilieva EV, , Kalluri H, McAllister D, Taherbhai MT, Esser ES, Pewin WP, Pulit-Penaloza JA, Prausnitz MR, Compans RW, Skountzou I. Improved immunogenicity of individual influenza vaccine components delivered with a novel dissolving microneedle patch stable at room temperature. Drug Deliv Transl Res. 2015;5:360–71. doi:10.1007/s13346-015-0228-0.
43. Rouphael NG, Paine M, Mosley R, Henry S, McAllister DV, Kalluri H, Pewin W, Frew PM, Yu T, Thornburg NJ, *et al*. The safety, immunogenicity, and acceptability of inactivated influenza vaccine delivered by microneedle patch (TIV-MNP 2015): a randomised, partly blinded, placebo-controlled, phase 1 trial. Lancet. 2017;390:649–58. doi:10.1016/S0140-6736(17)30575-5.
44. Hassert M, Wolf KJ, Schwetye KE, DiPaolo RJ, Brien JD, Pinto AK. CD4+T cells mediate protection against Zika associated severe disease in a mouse model of infection. PLoS Pathog. 2018;14:e1007237. doi:10.1371/journal.ppat.1007237.
45. Flammer J, Konieczka K, Bruno RM, Virdis A, Flammer AJ, Taddei S. The eye and the heart. Eur Heart J. 2013;34:1270–78. doi:10.1093/eurheartj/eht023.
46. Grabert K, McColl BW. Isolation and Phenotyping of Adult Mouse Microglial Cells. Methods Mol Biol. 2018;1784:77–86. doi:10.1007/978-1-4939-7837-3_7.
47. Lee JK, Tansey MG. Microglia isolation from adult mouse brain. Methods Mol Biol. 2013;1041:17–23. doi:10.1007/978-1-62703-520-0_3.
48. Mavigner M, Raper J, Kovacs-Balint Z, Gumber S, O'Neal JT, Bhaumik SK, Zhang X, Habib J, Mattingly C, McDonald CE, *et al*. Postnatal Zika virus infection is associated with persistent abnormalities in brain structure, function, and behavior in infant macaques. Sci Transl Med. 2018;10:eaao6975. doi:10.1126/scitranslmed.aao6975.
49. Taib T, Leconte C, Van Steenwinckel J, Cho AH, Palmier B, Torsello E, Lai Kuen R, Onyeomah S, Ecomard K, Benedetto C, *et al*. Neuroinflammation, myelin and behavior: temporal patterns following mild traumatic brain injury in mice. PLoS One. 2017;12:e0184811. doi:10.1371/journal.pone.0184811.
50. Brayton C, McBean NF, Watson J. JHU mouse pathobiology & phenotyping short course. Johns Hopkins University School of Medicine, Department of Molecular & Comparative Pathology; 2015. Vol. 4.
51. Drapeau E, Riad M, Kajiwara Y, Buxbaum JD. Behavioral phenotyping of an improved mouse model of phelan-mcdermid syndrome with a complete deletion of the shank3 gene. eNeuro. 2018:5. doi:10.1523/ENEURO.0046-18.2018.
52. Olsen CM, Childs DS, Stanwood GD, Winder DG. Operant sensation seeking requires metabotropic glutamate receptor 5 (mGluR5). PLoS One. 2010;5:e15085. doi:10.1371/journal.pone.0015085.
53. Ferrari G, Chauhan SK, Ueno H, Nallasamy N, Gandolfi S, Borges L, Dana R. A novel mouse model for neurotrophic keratopathy: trigeminal nerve stereotactic electrolysis through the brain. Invest Ophthalmol Vis Sci. 2011;52:2532–39. doi:10.1167/iovs.10-5688.
54. Ronca SE, Smith J, Koma T, Miller MM, Yun N, Dineley KT, Paessler S. Mouse Model of Neurological Complications Resulting from Encephalitic Alphavirus Infection. Front Microbiol. 2017;8:188. doi:10.3389/fmicb.2017.00188.
55. Blivis D, Haspel G, Mannes PZ, O'Donovan MJ, Iadarola MJ. Identification of a novel spinal nociceptive-motor gate control for Adelta pain stimuli in rats. Elife. 2017:6. doi:10.7554/eLife.23584.
56. Plotnikov MB, Chernysheva GA, Aliev OI, Smol'iakova VI, Fomina TI, Osipenko AN, Rydchenko VS, Anfinogenova YJ, Khlebnikov AI, Schepetkin IA, *et al*. Protective Effects of a New C-Jun N-terminal Kinase Inhibitor in the Model of Global Cerebral Ischemia in Rats. Molecules. 2019;24:1722. doi:10.3390/molecules24091722.
57. Neugebauer V, Han JS, Adwanikar H, Fu Y, Ji G. Techniques for assessing knee joint pain in arthritis. Mol Pain. 2007;3:8. doi:10.1186/1744-8069-3-8.
58. O'Leary TP, Robertson A, Chipman PH, Rafuse VF, Brown RE. Motor function deficits in the 12 month-old female 5xFAD mouse model of Alzheimer's disease. Behav Brain Res. 2018;337:256–63. doi:10.1016/j.bbr.2017.09.009.
59. Fink SL, Cookson BT. Apoptosis, pyroptosis, and necrosis: mechanistic description of dead and dying eukaryotic cells. Infect Immun. 2005;73:1907–16. doi:10.1128/IAI.73.4.1907-1916.2005.
60. Miao EA, Rajan JV, Aderem A. Caspase-1-induced pyroptotic cell death. Immunol Rev. 2011;243:206–14. doi:10.1111/j.1600-065X.2011.01044.x.
61. Yang M, Antoine DJ, Weemhoff JL, Jenkins RE, Farhood A, Park BK, Jaeschke H. Biomarkers distinguish apoptotic and necrotic cell death during hepatic ischemia/reperfusion injury in mice. Liver Transpl. 2014;20:1372–82. doi:10.1002/lt.23958.
62. Lourenco T, Paes de Faria J, Bippes CA, Maia J, Lopes-da-Silva JA, Relvas JB, Grãos M. Modulation of oligodendrocyte differentiation and maturation by combined biochemical and mechanical cues. Sci Rep. 2016;6:21563. doi:10.1038/srep21563.
63. Esser ES, Romanyuk A, Vassilieva EV, Jacob J, Prausnitz MR, Compans RW, Skountzou I. Tetanus vaccination with a dissolving microneedle patch confers protective immune responses in pregnancy. J Control Release. 2016;236:47–56. doi:10.1016/j.jconrel.2016.06.026.
64. Titilope Oduyebo MKDP, Walke HT, Reagan-Steiner S, Reagan-Steiner S, Lathrop E, Rabe IB, Kuhnert-Tallman WL, Martin SW,

Walker AT, Gregory CJ, *et al*. Update: interim Guidance for Health Care Providers Caring for Pregnant Women with Possible Zika Virus Exposure — united States (Including U.S. Territories), July 2017. MMWR Surveill Summ. 2017;66:781–93. doi:10.15585/mmwr.mm6629e1.
65. Triolo D, Dina G, Taveggia C, Vaccari I, Porrello E, Rivellini C, Domi T, La Marca R, Cerri F, Bolino A, *et al*. Vimentin regulates peripheral nerve myelination. Development. 2012;139:1359–67. doi:10.1242/dev.072371.
66. Naik GS, Meena A, Reddy BK, Mridula R, Jabeen S, Borgohain R. Anti-ganglioside antibodies profile in Guillain-Barre syndrome: correlation with clinical features, electrophysiological pattern, and outcome. Neurol India. 2017;65:1001–05. doi:10.4103/neuroindia.NI_1226_15.
67. Guevara JG, Agarwal-Sinha S. Ocular abnormalities in congenital Zika syndrome: a case report, and review of the literature. J Med Case Rep. 2018;12:161. doi:10.1186/s13256-018-1679-y.
68. Ventura CV, Ventura LO. Ophthalmologic manifestations associated with Zika virus infection. Pediatrics. 2018;141:S161–S166. doi:10.1542/peds.2017-2038E.
69. Frankola KA, Greig NH, Luo W, Targeting TD. TNF-alpha to elucidate and ameliorate neuroinflammation in neurodegenerative diseases. CNS Neurol Disord Drug Targets. 2011;10:391–403. doi:10.2174/187152711794653751.
70. Wang P, Dai J, Bai F, Kong K-F, Wong SJ, Montgomery RR, Madri JA, Fikrig E. Matrix metalloproteinase 9 facilitates West Nile virus entry into the brain. J Virol. 2008;82:8978–85. doi:10.1128/JVI.00314-08.
71. Mori T, Miyamoto T, Yoshida H, Asakawa M, Kawasumi M, Kobayashi T, Morioka H, Chiba K, Toyama Y, Yoshimura A, *et al*. IL-1beta and TNFalpha-initiated IL-6-STAT3 pathway is critical in mediating inflammatory cytokines and RANKL expression in inflammatory arthritis. Int Immunol. 2011;23:701–12. doi:10.1093/intimm/dxr077.
72. Samad TA, Moore KA, Sapirstein A, Billet S, Allchorne A, Poole S, Bonventre JV, Woolf CJ. Interleukin-1beta-mediated induction of Cox-2 in the CNS contributes to inflammatory pain hypersensitivity. Nature. 2001;410:471–75. doi:10.1038/35068566.
73. Ashley SL, Pretto CD, Stier MT, Kadiyala P, Castro-Jorge L, Hsu T-H, Doherty R, Carnahan KE, Castro MG, Lowenstein PR, *et al*. Matrix metalloproteinase activity in infections by an encephalitic virus, mouse adenovirus type 1. J Virol. 2017;91. doi:10.1128/JVI.01412-16.
74. Konnecke H, Bechmann I. The role of microglia and matrix metalloproteinases involvement in neuroinflammation and gliomas. Clin Dev Immunol. 2013;2013:914104. doi:10.1155/2013/914104.
75. Rempe RG, Hartz AMS, Bauer B. Matrix metalloproteinases in the brain and blood-brain barrier: versatile breakers and makers. J Cereb Blood Flow Metab. 2016;36:1481–507. doi:10.1177/0271678X16655551.
76. Song J, Wu C, Korpos E, Zhang X, Agrawal S, Wang Y, Faber C, Schäfers M, Körner H, Opdenakker G, *et al*. Focal MMP-2 and MMP-9 activity at the blood-brain barrier promotes chemokine-induced leukocyte migration. Cell Rep. 2015;10:1040–54. doi:10.1016/j.celrep.2015.01.037.
77. DiSabato DJ, Quan N, Godbout JP. Neuroinflammation: the devil is in the details. J Neurochem. 2016;139(Suppl 2):136–53. doi:10.1111/jnc.13607.
78. Baker BJ, Akhtar LN, Benveniste EN. SOCS1 and SOCS3 in the control of CNS immunity. Trends Immunol. 2009;30:392–400. doi:10.1016/j.it.2009.07.001.
79. Burmeister AR, Marriott I. The Interleukin-10 Family of Cytokines and Their Role in the CNS. Front Cell Neurosci. 2018;12:458. doi:10.3389/fncel.2018.00458.
80. Khaiboullina S, Uppal T, Kletenkov K, St. Jeor SC, Garanina E, Rizvanov A, Verma SC. Transcriptome profiling reveals pro-inflammatory cytokines and matrix metalloproteinase activation in Zika virus infected human umbilical vein endothelial cells. Front Pharmacol. 2019;10:642. doi:10.3389/fphar.2019.00642.
81. Nakamura R, Sene A, Santeford A, Gdoura A, Kubota S, Zapata N, Apte RS. IL10-driven STAT3 signalling in senescent macrophages promotes pathological eye angiogenesis. Nat Commun. 2015;6:7847. doi:10.1038/ncomms8847.
82. Ponomarenko NA, Durova OM, Vorobiev II, Belogurov AA, Kurkova IN, Petrenko AG, Telegin GB, Suchkov SV, Kiselev SL, Lagarkova MA, *et al*. Autoantibodies to myelin basic protein catalyze site-specific degradation of their antigen. Proc Natl Acad Sci U S A. 2006;103:281–86. doi:10.1073/pnas.0509849103.
83. Al-Fifi YSY, Kadkhoda K, Drebot M, Wudel B, Bow EJ The first case report of West Nile virus-induced acute flaccid quadriplegia in Canada. *Case Rep Infect Dis*. 2018;2018;4361706. doi:10.1155/2018/4361706.
84. Van Gerpen JA. Neurologic sequelae of west nile virus infection. Ochsner J. 2003;5:18–20.
85. Komagamine T, Matsuno K, Sakumoto Y, Takahashi H, Kokubun N, Yuki N, Hirata K. Immunohistochemical localization of the GM1, GD1a, GD1b and GQ1b gangliosides in the neuronal endings of rat muscle spindles. Arch Histol Cytol. 2013;74:31–40. doi:10.1679/aohc.74.31.
86. Kopper TJ, Gensel JC. Myelin as an inflammatory mediator: myelin interactions with complement, macrophages, and microglia in spinal cord injury. J Neurosci Res. 2018;96:969–77. doi:10.1002/jnr.24114.